AN EXPERIMENTAL INVESTIGATION OF MULTI-RING UNDER QUASI-STATIC AND DYNAMIC LOADING

VINESH A/L UNAKRISHNAN

UNIVERSITI TEKNIKAL MALAYSIA MELAKA

AN EXPERIMENTAL INVESTIGATION OF MULTI-RING UNDER QUASI-STATIC AND DYNAMIC LOADING

VINESH A/L UNAKRISHNAN

A report submitted

in fulfillment of the requirements for the degree of

Bachelor of Mechanical Engineering (Structure and Material)

Faculty of Mechanical Engineering

UNIVERSITI TEKNIKAL MALAYSIA MELAKA

2017

DECLARATION

I declare that this project report entitled “An experimental investigation of multi-ring under quasi-static loading and dynamic loading” is the result of my own work except as cited in the references

Signature : ……………………………….

Name : ……………………………….

Date : ……………………………......

APPROVAL

I hereby declare that I have read this project report and in my opinion this report is sufficient in terms of scope and quality for the award of the degree of Bachelor of Mechanical Engineering (Structure & Materials).

Signature :: ....

Name of Supervisor : ....

Date : ....

DEDICATION

To my beloved mother and father

ABSTRACT

Energy absorbers play an important role in reducing the amount of impact subjected to structure to ensure the safety of the human in that structure. Rings are good energy absorbers since it is low in cost and addition of internal rings make it a better energy absorber when subjected to lateral loading. Two types of experiment were conducted which were the tensile test and compression test. Tensile test was conducted to determine the mechanical properties of the mild steel and compression test consisting of quasi-static loading and dynamic loading was conducted onto the ring to determine the energy absorbing capacity. Comparisons were made experimentally between multi ring and single ring under quasi-static loading and dynamic loading and motion recording were done using a camera for the respective experiments. A mild steel multi-ring consisting of four internal rings were fabricated in this project. The energy absorbing capacity was obtained from the area under the graph until the plateau zone. It was proven that multi-ring has a better energy absorbing capacity than single ring when it was quasi-statically loaded and dynamically loaded since there is an addition of constraints.

ABSTRAK

Penyerap tenaga memainkan peranan yang amat penting dalam mengurangkan kesan impak yang dikenakan pada sesuatu struktur untuk memastikan keselamatan manusia di dalam struktur tersebut. Cincin adalah penyerap tenaga yang baik kerana ianya murah dan penambahan cincin secara dalaman dapat meningkatkan kapasiti penyerapan tenaga. Dua jenis eksperimen telah dijalankan iaitu ujian regangan dan mampatan. Ujian regangan telah dijalankan untuk mengetahui ciri-ciri mekanikal bahan yang digunakan dan ujian mampatan dijalankan untuk mengetahui kapasiti penyerapan tenaga cincin. Perbandingan telah dibuat secara eksperimen antara cincin tunggal dan cincin berbilang dimana beban kuasi-statik dan beban dinamik telah dikenakan dan pergerakan impak telah direkodkan menggunakan kamera untuk setiap eksperimen. Cincin berbilang tersebut mempunyai empat cincin dalaman yang diperbuat daripada keluli lembut. Kapasiti penyerapan tenaga telah diperoleh daripada keluasan graf sehingga zon plateau. Ianya telah terbukti bahawa cincin berbilang mempunyai kapasiti penyerapan tenaga yang lebih tinggi daripada cincin tunggal apabila dikenakan beban kuasi-statik dan beban dinamik.

ACKNOWLEDGEMENT

First and foremost I would like to thank God the almighty for providing me the health and wellbeing and also for allowing me to complete this project in a smooth manner. My deepest appreciation to my supervisor, Prof Dr. Md Radzai Bin Said for giving me an opportunity to conduct this final year project under his supervision. His guidance and encouragement was the reason behind the completion of this project. I would like to extend my sincere thanks to him for sharing his expertise in leading me in this project.

My sincere thank you to my family and friends for their continuous support and love on me throughout. I am also grateful to the lab technicians, Mr.Faizal, Mr Wan, and Mr.Faizol for assisting me in the experimental works that were carried out during this project.

CONTENT

LIST OF TABLES

LIST OF FIGURES

LIST OF ABBEREVIATIONS

RSM	Response surface method
SEA	specific energy absorption
CFE	crushing force efficiency
MIG	Metal inert gas

LIST OF SYMBOL

E	=	Modulus of elasticity/Energy absorbed
σ	=	Engineering stress
ε	=	Engineering strain
G	=	Modulus of rigidity
F	=	Force/Force indentation stroke
L	=	Initial length
A	=	Area
Δx	=	Transverse displacement
$\dot{\varepsilon}$	=	Strain rate
$\dot{\sigma}$	=	Stress rate
P	=	Flattening force
δ	=	Deflection
P_k	=	Peak crushing force
P_m	=	Mean crushing force
σ_v	=	Standard quasi-static tensile characteristic of a given material

M_0 = Moment per unit length

σ_{od} = Dynamic yield stress

σ_o = Static yield stress

CHAPTER 1

INTRODUCTION

1.1 BACKGROUND

Energy absorbers has been given much of an attention to researchers around the world because of its ability to protect the occupant or reducing the injury of the occupant placed in a particular structure. Studies regarding crashworthiness have great attention to the behavior of thin-walled structures, which is used as energy absorbers in fields such as aeronautical and automobile (Li et al., 2013). In order to further understand the energy absorption of a structure, understanding of materials engineering, structural mechanics, impact mechanics, and theory of plasticity is important. Usually thin-walled tubes of different geometry and materials are used to absorb kinetic energy through plastic material deformation. There are many ways of destroying thin-walled tubes in order to analyze the energy absorbed such as lateral compression, lateral indentation, axial crushing, tube inversion and tube splitting. (Baroutaji et al., 2016). Axially loaded structures have drawn attention to many researchers since axial crushing has high energy absorbing capacity. However, its disadvantage is that it has very large fluctuations of the collapse load about a mean load and unstable deformation mode. This project focuses on the effects of lateral loading on short circular tube. Energy absorbing capacity of laterally loaded structures are higher compared to laterally indented structures because bending collapse mode generated from lateral loading results in a smooth force-deflection response. Besides, it does not undergo any unstable deformation mode (Baroutaji et al., 2015). A research study has found out that circular tube structures under lateral quasi-static loading using response surface method (RSM) and showed that specific energy could be increased by increasing the thickness and reducing the diameter of the tubes (AlaviNia and Chahardoli, 2016). On the other hand, a study conducted shows that an elliptical ring has greater energy absorbing capacity compared to circular ring because of its higher displacement stroke (Morris et al., 2007). The effects multi-ring structure subjected to laterally quasi-static loading and laterally dynamic loading will be studied throughout this project.

1.2 PROBLEM STATEMENT

Energy absorption plays a vital role in engineering structures and fields such as in the automobile and aeronautical industries. These impact energy absorption devices are highly responsible in ensuring the safety and life of human beings. Besides, impact energy absorption devices are used to avoid high impact loads on commercial goods packages. In the current world, it is important for a designer to design an impact energy absorbing device which could limit loads and deceleration on the structure and occupants. Circular rings are used as thin-walled energy absorbers since it is low in cost compared to solid tubular energy absorbers and is widely used in crash barriers. Multi-circular rings increases the energy absorption capacity when impact is exerted on a structure compared to a single ring.

1.3 OBJECTIVE

The objectives of this project are as follows:

1. To study the comparison of energy absorption between lateral quasi-static loading and lateral dynamic loading on a multi-ring structure.
2. To observe the deforming mode of multi-ring subjected to quasi-static and dynamic loading.
3. To study the load-displacement characteristics and energy absorption.

1.4 SCOPE OF PROJECT

This project focuses on the experimental work that will be conducted on metal circular multi-ring which will be laterally compressed. The mode is compared between quasi-static and dynamic loading with various arrangements of smaller rings. Besides that, observation and studies will be made on the deforming mode, collapse load, densification and energy absorbed on the circular multi-ring and single ring.

CHAPTER 2

LITERATURE REVIEW

2.1 Introduction

Literature review is a study survey conducted on the field of a particular chosen area of interest by a researcher. This literature review comprises of basic mechanical properties involved in this project, a review of the energy absorber, a review of laterally loaded circular thin-walled structure, and brief explanation of quasi-static and dynamic loading.

2.2 Modulus of elasticity

Modulus of elasticity, E, also known as Young's modulus, is the slope at the initial part of the stress-strain curve (Moosbrugger, 2002). The equation is shown as below

$$E = \frac{\sigma}{\varepsilon} \qquad \text{Eq.(1)}$$

Where σ, is engineering stress and ε, is engineering strain. A measure of stiffness is what defines modulus of elasticity. A high value of modulus of elasticity causes the slope to be more abrupt and results in smaller the elastic strain for the applied stress. The Young's modulus is determined by the binding forces between atoms. Because these forces cannot be changed without changing the basic nature of the material, the modulus of elasticity is one of the most structure-insensitive of the mechanical properties. (Moosbrugger, 2002)

2.3 Modulus of rigidity

Shear modulus or modulus of rigidity, G or sometimes denoted as S or μ is the ratio of shear stress to shear strain. (Gold, 1987)

$$G = \frac{Fl}{A\Delta x} \qquad \text{Eq.(2)}$$

Whereby F is the force acting on the object, *l* is the initial length, A is the area where the force acts on and Δx is the transverse displacement.

2.4 Yield strength

Yield strength is also known as the stress at which the first load peak occurs during tensile test. Besides that, it is also defined as the stress to cause a predetermined amount of total strain. It is almost/approximately true that yield strength of metals are the same when it is subjected to compression loading or tension loading. (Murray, 1997). Yield strength is the transition point of elastic deformation to plastic deformation in a stress-strain curve. Yield behavior in pure shear in ductile metals is clearly defined by the von Mises criterion. According to this criterion, shear stress to cause yielding will be about 57% of the axial stress to cause yielding. Typically most ductile materials yield between 55% and 60% of the yield strength. (Murray, 1997).

2.5 Ultimate tensile strength

Ultimate tensile strength, σ_u is the maximum stress that could be withstand by a material when subjected to tensile load. Necking of the specimen occurs when the stress approaches ultimate tensile strength causing the cross-sectional area to decrease. This proves that true stress to be higher than the engineering stress. True stress is defined by force divided by the actual specimen cross section area. Engineering stress is defined as the force per-unit initial cross section area (Chung, 2007). The typical stress-strain graph of a ductile material is shown in Figure 2.1.

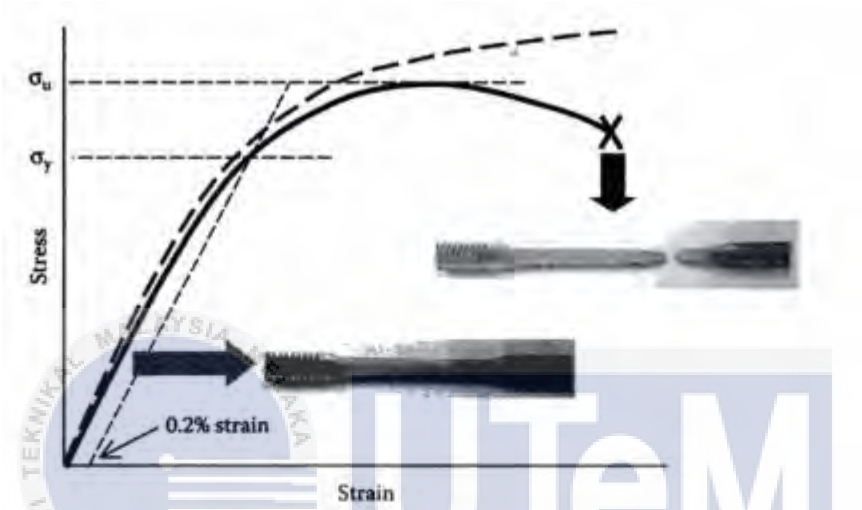

Figure 2.1 Typical stress-strain graph for ductile material

2.6 Energy absorber

Energy absorbers plays a very important role in converting totally or partially kinetic energy into other forms of energy such as pressure energy, elastic strain energy or plastic deformation energy. A designer aims to design a collapsible energy absorber which could absorb the kinetic energy of the impact whereby it is irreversible. This ensures the safety of the occupants/human. Magnitude, and how the loads are applied, transmission rates, deformation pattern and material properties are the factors affecting the conversion of kinetic energy into plastic deformation. Circular tubes, circular rings, square tubes, corrugated tubes, multi-corner tubes, frusta, struts, honeycomb cells, and sandwich plates are the examples of deformable energy absorbers (Alghamdi, 2000).

2.7 Quasi-static loading and Dynamic loading

The speed of a loading to an object is defined by loading rate. It also can be expressed in different forms, which are usually expressed by strain rate, $\dot{\varepsilon}$ or by stress rate, $\dot{\sigma}$. (Zhang, 2016) . The expressions or equations on strain rate and stress rate are defined as below:

$$\dot{\varepsilon} = \frac{d\varepsilon}{dt} \qquad \text{Eq.(3)}$$

$$\dot{\sigma} = \frac{d\sigma}{dt} \qquad \text{Eq.(4)}$$

Loading through stress waves is included as dynamic loading. The loading rates corresponding to dynamic loading are approximately in the range of

$\dot{\varepsilon} > 10^1 s^{-1}$

Static or quasi-static loading rates has very small and no stress waves dealt with and has loading rates in the range of

$\dot{\varepsilon} < 10^1 s^{-1}$

Comparisons between quasi-static and dynamic loading is important because the effect of dynamic loading can be resolved and evaluated (Baroutaji et al., 2016)

When dynamic loading is subjected to a structure, deformation which occurs on the structure will be fast causing the presence of high strain rates (Lu & Yu, 2003). Besides, it could also cause a quick gain in stress and particle velocity at the points on the loaded surface. On the other hand, when dynamic load is acted upon a structure, the stress waves in its transverse direction also ends rapidly. Then, as the structure deforms, the inertia of that particular component becomes the factor of the dynamic performance (Jones, 1989).

Figure 2.2 Elastic, perfectly plastic model (Lu & Yu, 2003)

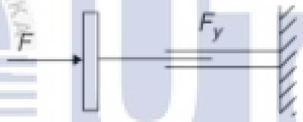

Figure 2.3 Rigid, perfectly plastic model (Lu & Yu, 2003)

Figure 2.2 and Figure 2.3 shows the significant difference of dynamic loading and quasi-static loading and its effect on inertia. If the mass shown in the figure above is a concentrated mass, the rigid, perfectly plastic model (Figure 2.3) will not be able to withstand any quasi-static load greater than F_y, whereby F_y is the limit force of the structural model.

For many structural impact situations, the Copper-Symonds relation has been used for rate-dependent constitutive equations of engineering materials. The equation below is used mainly for rigid, perfectly plastic materials.

$$\frac{\sigma_{0d}}{\sigma_0} = 1 + \left(\frac{\dot{\varepsilon}}{B}\right)^{1/q} \qquad \dot{\varepsilon} > 0 \qquad \text{Eq.(5)}$$

Where, σ_{0d} is the dynamic yield stress, σ_0 is the static yield stress, $\dot{\varepsilon}$ is the strain-rate, and B and q are the material constant. The static yield stress, σ_0 could be determined from the uniaxial tensile test, whereas the dynamic yield stress, σ_{0d} is calculated from the equation Eq.(5). This shows that the dynamic yield stress is dependent on the strain-rate. The representative values of B and q are shown in Table 2.1. The values shown are for strain,

ε = 0.05.

Table 3.1 Parameters representative rate-sensitive materials (Lu & Yu, 2003)

Material	**B (s^{-1})**	**q**	**B_q(s^{-1})**	**Reference**
Mild steel	40	5	65	Forrestal and Wesenberg,1977
Stainless steel	100	10	160	Forrestal and Sagartz, 1978
Titanium (Ti 50A)	120	9	195	Stronge and Yu, 1993
Aluminium 6061-T6	1.70×10^6	4	2.72×10^6	Symonds, 1965
Aluminium 3003-H14	0.27×10^6	8	0.44×10^6	Bodner and Speirs, 1963

2.8 Laterally loaded circular thin-walled structures

Based on a research conducted by (Khalil et al., 2014) on flat and hemispherical type of indentor and flat and hemispherical type of shell, the bending force becomes lower as the indentor strokes caused by the large hinge radius in the deformation pattern. The force applied on the shells is 1.5 times higher than in quasi-static test. This makes the energy absorbed in impact deformation is greater than in quasi-static loading. Besides that, it was also found that application of in-plane compressive stress gives an improvement in energy absorbtion performance. The energy absorbed, E is determined by intergrating the force variation, F with indentation stroke.

$$E = \int_{H_0}^{Hf} F(x)dx \qquad \text{Eq.(6)}$$

Based on a review conducted by (Alghamdi, 2000) , a simple rigid plastic analysis for lateral compression gives a flattening force, P by:

$$P = \frac{4Yt^2L}{\sqrt{3}D(1-(\delta/D)^2)^{1/2}} \qquad \text{Eq.(7)}$$

Where L is the length of tube, D is the diameter and δ is the deflection.

Lateral loading has not been given much attention in research works compared to axial and oblique loading. The long tubes under lateral loading undergoes bending collapse mode when force is generated. For short tubes (rings), they undergo plastic bending at plastic hinges lines. This causes plastic strain to be concentrated and causes energy dissipation at the plastic hinge lines (Tran, 2016). Besides that the crushing force efficiency (CFE) is given by the equation below:

$$\mathrm{CFE} = \frac{P_k}{P_m} \qquad \text{Eq.(8)}$$

Where P_k is the peak crushing force and P_m is the mean crushing force.

Comparing with laterally loaded tubes and axially loaded tubes, energy absorbed by the laterally loaded tubes are much lower than the axially loaded tubes. Energy absorbing capacity of this laterally loaded tubes can be increased by allowing the tubes to deform in many ways. For this to occur, involvement of plastic hinges are needed and it could be done by constraining the tubes at their sides (Reddy and Reid, 1978). Figure 2.4 and Figure 2.5 shows the experimental arrangements for constrained tubes with friction and without friction respectively by (Reddy and Reid, 1978).

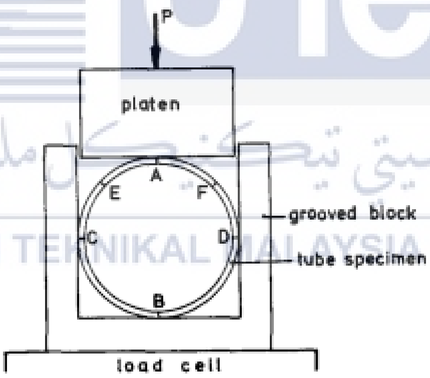

Figure 2.4 Experimental arrangements for constrained tubes with friction (Reddy and Reid, 1978)

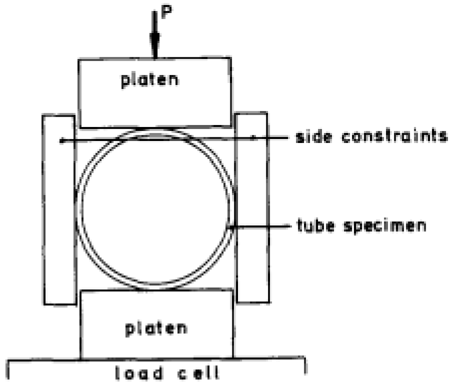

Figure 2.5 Experimental arrangements for tubes without friction (Reddy & Reid, 1978)

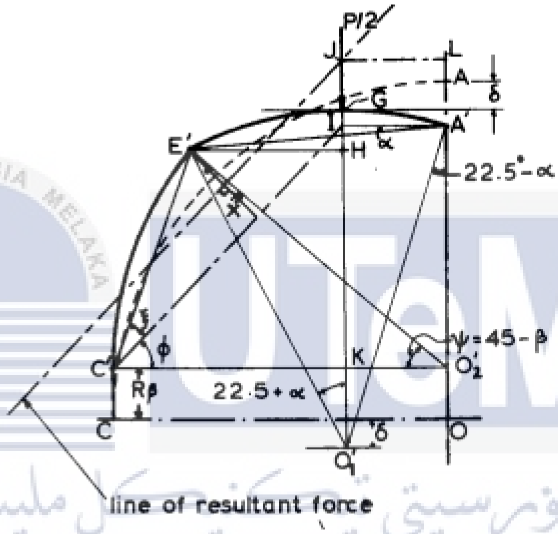

Figure 2.6 Geometry of the deforming of the left quadrant in stage one for constrained tube (Reddy & Reid, 1978)

Based on the experiment conducted by (Reddy & Reid, 1978), it was determined that the tubes that are laterally loaded with constraints has energy absorption capacity which are three times higher than the free system. Figure 2.6 shows the geometry of the deforming of the left quadrant in stage one for constrained tube by (Reddy & Reid, 1978).

Head on collision of vehicles has been a common study by researchers. Now, energy absorber when a vehicle is subjected to side impact, also has been the area of research for today's researchers. Based on a research conducted by (Reid and Drew, 1983) steel tubes which were attached with tension member across the diameter which also acts as a reinforcement, subjected on lateral loading, shows that high amount of energy absorption occurs at a bracing angle of 15°. Figure 2.7 and Figure 2.8 shows the braced metal tube (single wired) and different deformations of single braced tube at angle of 15° respectively by (Reid and Drew, 1983).

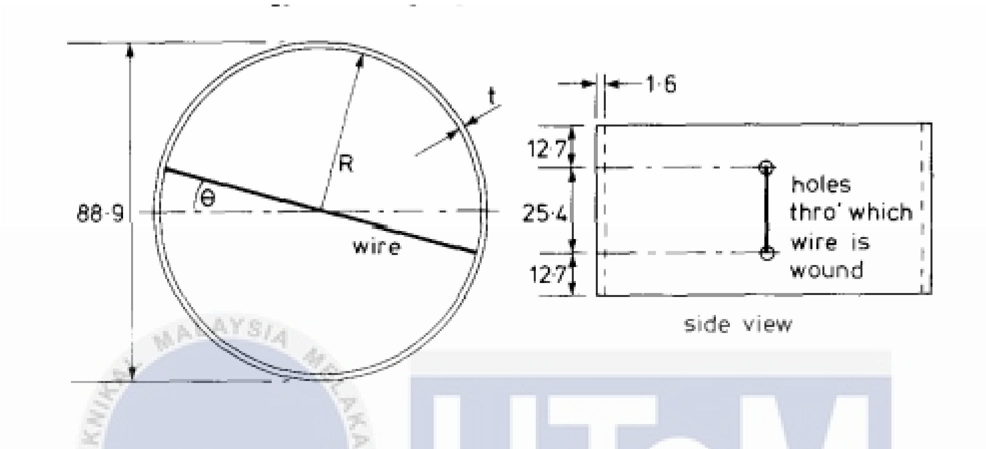

Figure 2.7 Braced metal tube (single wired) (Reid and Drew, 1983)

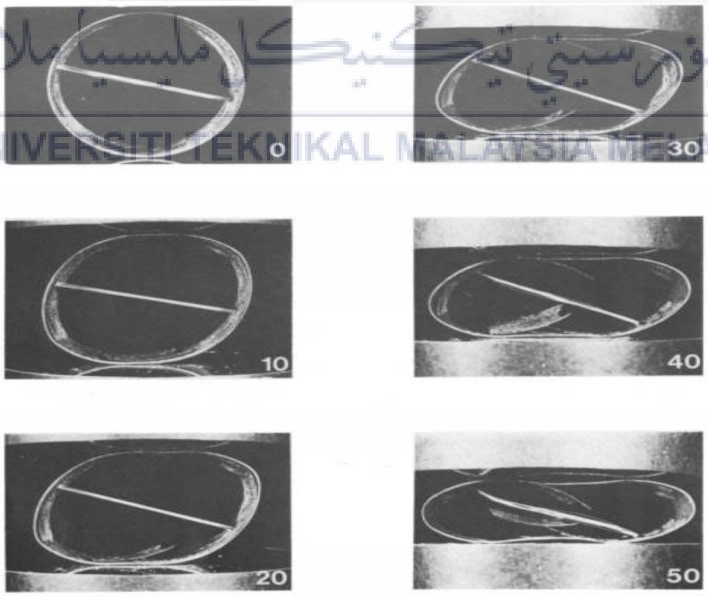

Figure 2.8 Different deformations of single braced tube at angle of 15° (Reid & Drew, 1983)

A comparison study between numerical method and experimental method made by (Baroutaji et al., 2015) shows that, the collapse mode is plastic bending around plastic hinges when a thin-walled circular tube is subjected to quasi-static lateral loading. Besides that, the study also shows that the specific energy absorbing (SEA) capacity could be increased by if the thickness and diameter of the tube is thicker and smaller respectively. Energy absorbing capacity of a circular tube under lateral loading could be increased by decreasing the width and diameter and increasing the thickness. Figure 2.9 and Figure 2.10 shows the comparison between experimental and numerical deformation under lateral loading and geometry of a short circular tube respectively which was studied by (Baroutaji et al., 2015).

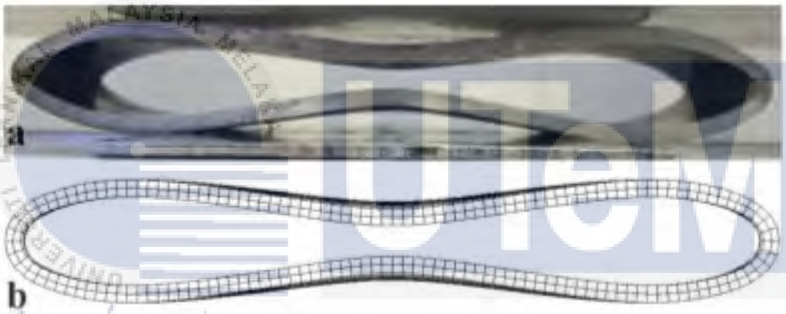

Figure 2.9 Comparison between experimental and numerical deformation under lateral loading (Baroutaji et al., 2015)

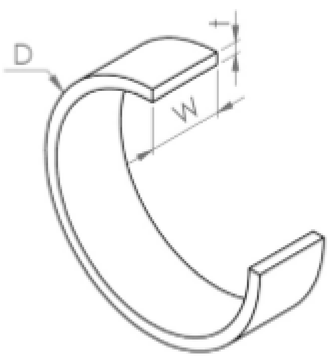

Figure 2.10 Geometry of a short circular tube (Baroutaji et al., 2015)

Nested circular tubes has gaps between them to allow them to deform consecutively as loading is increased. This causes a non-monotonic increase in force in the deformation. For internally nested tubes with the same diameter, it is assumed/expected that the tubes deform together, but this could not be achieved experimentally. The reason is because symmetrical collapse mode and simultaneous deformation could not achieved when the circular nested tubes were subjected to lateral loading (Baroutaji et al., 2016). Figure 2.11 shows the deformation of internally nested tubes with similar internal tube diameter where the experiment was conducted by (Baroutaji et al., 2016).

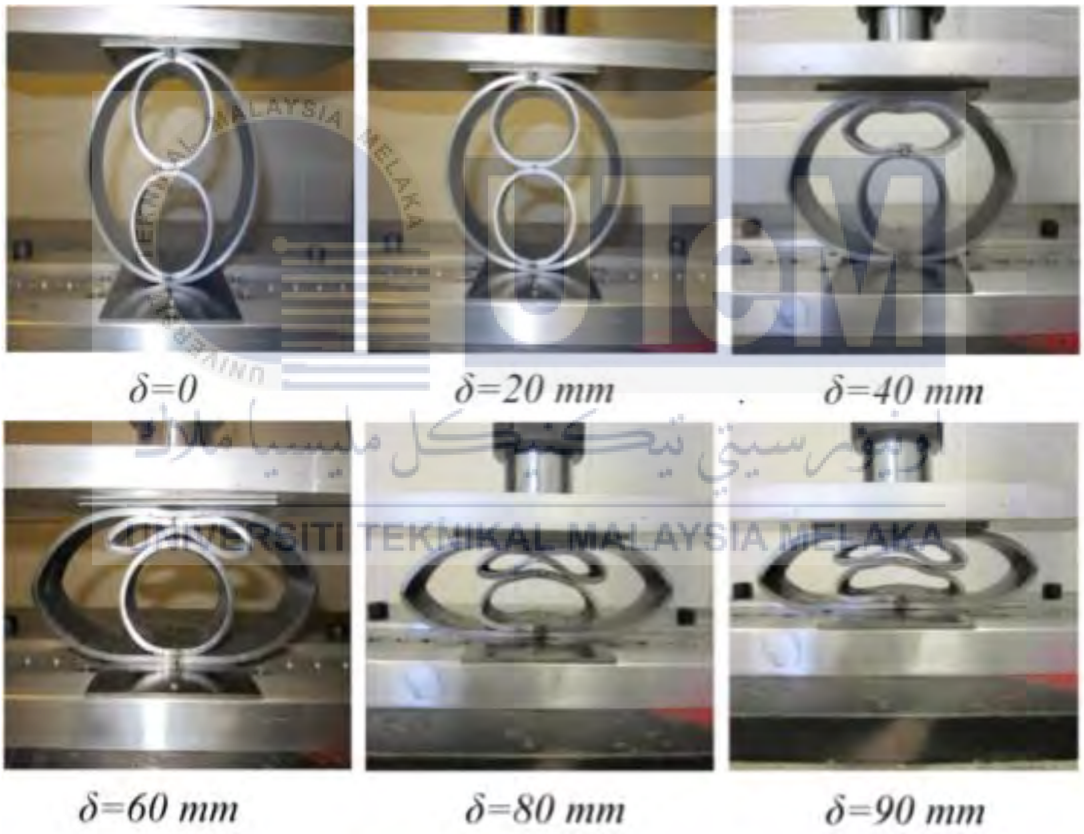

Figure 2.11 Deformation of internally nested tubes with similar internal tube diameter (Baroutaji et al., 2016)

In the book of Energy Absorption of Structures and Materials by (.Lu & Yu, 2003), it was stated that a total of four plastic hinges could collapse a ring under compression of two flat plates. Besides that, there are two modes of collapse when ring is subjected to lateral loading, which are by mode researched by (Burton and Craig, 1963; de Runtz and Hodge, 1963). The mode proposed by de Runtz and Hodge is as shown in Figure 2.12 has four stationary plastic hinges and is suitable to be used for rings made of mild steel, having an upper and lower yield point.

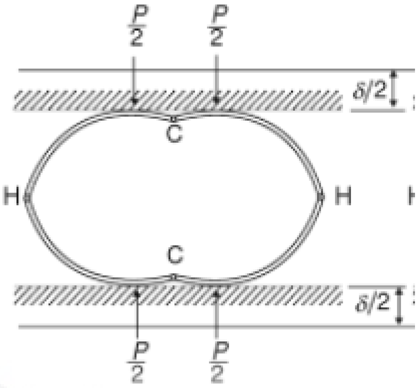

Figure 2.12 the mechanics of collapse researched/proposed by de Runtz and Hodge (1963)

On the other hand, the mode proposed by Burton and Craig as shown in Figure 2.13, has straightening of the ring at the moving contact point.

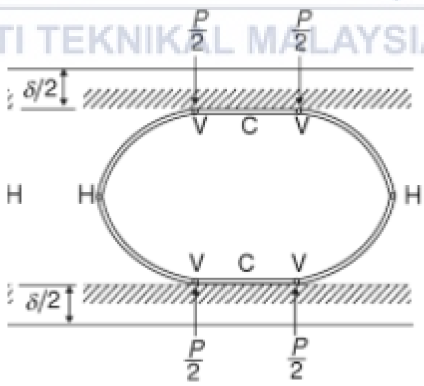

Figure 2.13 the mechanics of collapse researched/proposed by Burton and Craig (1963)

Both the collapse modes has similar deforming segments as shown in Figure 2.14 and hence has the similar initial collapse load equation.

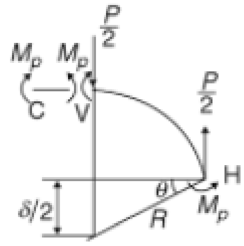

Figure 2.14 Deforming segment of a quadrant of a ring

$$P = \frac{4\,M_0}{R\,cos\,\theta}$$ Eq.(9)

Where M_0 is the moment per unit length R is the radius of the ring and θ is the angle of deformation. When the angle of deformation is zero, this indicates that the ring starts to deform, and the initial collapse load, P_0 to cause deformation is shown in the equation below.

$$P_0 = \frac{4M_0}{R}$$ Eq.(10)

From the equilibrium based on the deforming segment in Figure 2.12, the deformation geometry, δ is as below

$$\delta = 2\,R \sin\,\theta$$ Eq.(11)

The combination of both Eq.(9) and Eq.(10) gives an equation of as shown below:

$$P = \frac{\sigma t^2 L}{D[1-(\delta/D)^2]^{1/2}}$$ Eq.(12)

Where σ is the yield stress, L is the width of ring, t is thickness of ring, δ is the deflection/deformation of ring when subjected to lateral loading and D is the diameter of the ring. From Eq.(11) it proves that deflection/deformation increases as the lateral load subjected on a ring increases. Yield stress, σ is taken from the uniaxial tensile test and is taken as $2\sqrt{3}$ of the yield stress if the diameter of the tube is shorter than its length.

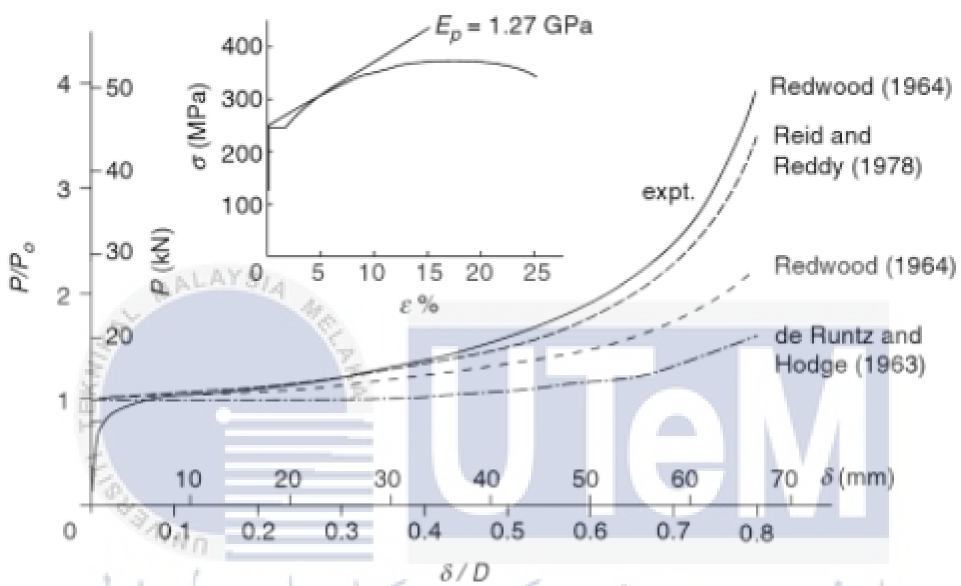

Figure 2.15 Non-dimensional load versus displacement curves from experiments and theories (Reid, 1983)

Figure 2.15 shows that the de Runtz and Hodge method is lower than the other researchers experimental results. This may due to the increase of plastic bending moment resistance as deformation increase. Besides, it may also due to plastic deformation which is not concentrated at the plastic hinge.

CHAPTER 3

METHODOLOGY

3.1 Introduction

This chapter describes the method used in obtaining the data for the energy absorption of a multi-ring when subjected to laterally quasi-static and laterally dynamic loading. The flow chart of this project is shown in Figure 3.1. The general work flow of this project are conducting tensile test to obtain the mechanical properties of the material used, proposing the design/position of rings, fabricating the multi-ring and conducting the compression test which includes quasi-static loading test and dynamic loading test.

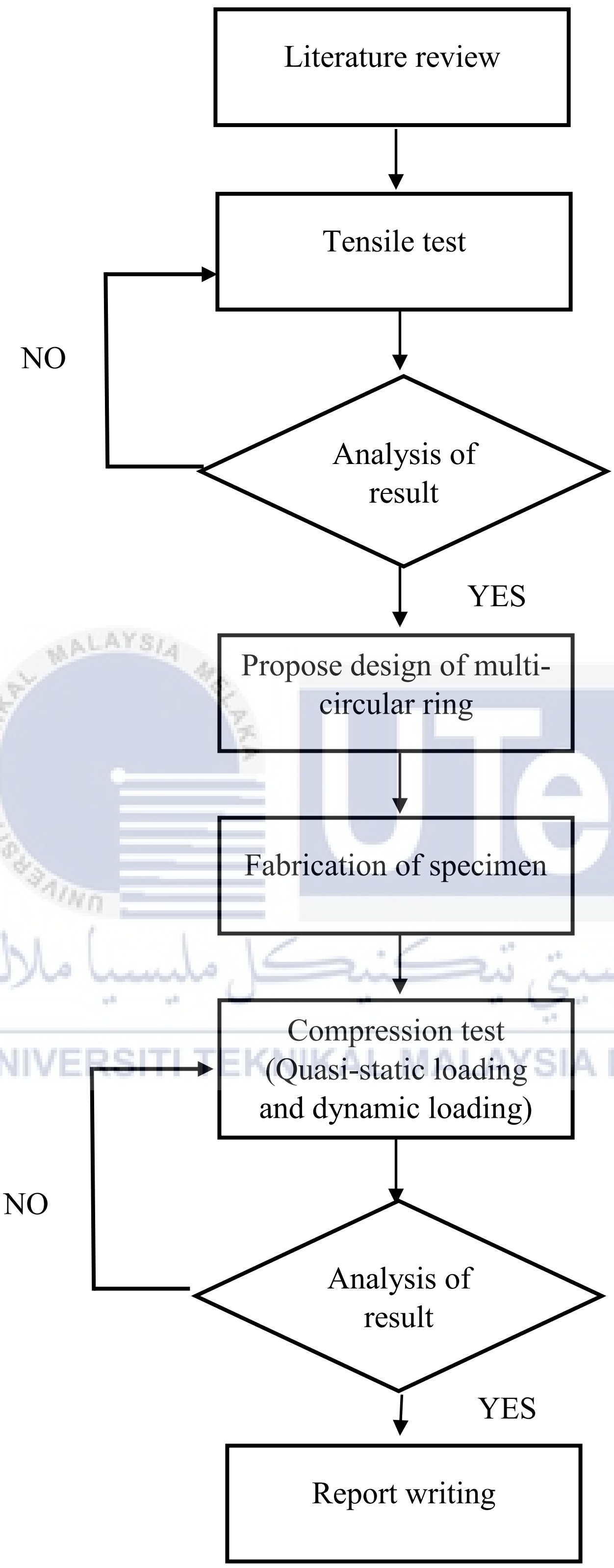

Figure 3.1 Flow chart of the project

In order to follow the flow of work, Gantt charts were prepared for the first and second semester in order to properly manage the project (Appendix A1 and Appendix A2). These Gantt charts were another way of getting a handle on the future. It makes the project to run effectively on the allocated time. Basically, the design of the ring position and tensile test was conducted doing the first half of the project. Whereas, fabrication of the ring specimen, quasi-static loading test and dynamic loading test were conducted on the second half of the project.

3.2 Proposing design of multi-ring

The proposed design/position of the multi-ring is shown below on Figure 3.2. SolidWorks version 2013 software was used as the computer aided drawing in designing this multi-ring. Four internal circular ring with the same the diameter and thickness was used as the position of the nested circular tube. Each internal ring are positioned together, creating tangential curves with each other leaving no space between the internal circular tubes. From the drawing made, it shows that the outer ring has 43mm of diameter and the internal ring has a diameter of 16mm. Both internal and outer ring has similar thickness of 2mm.

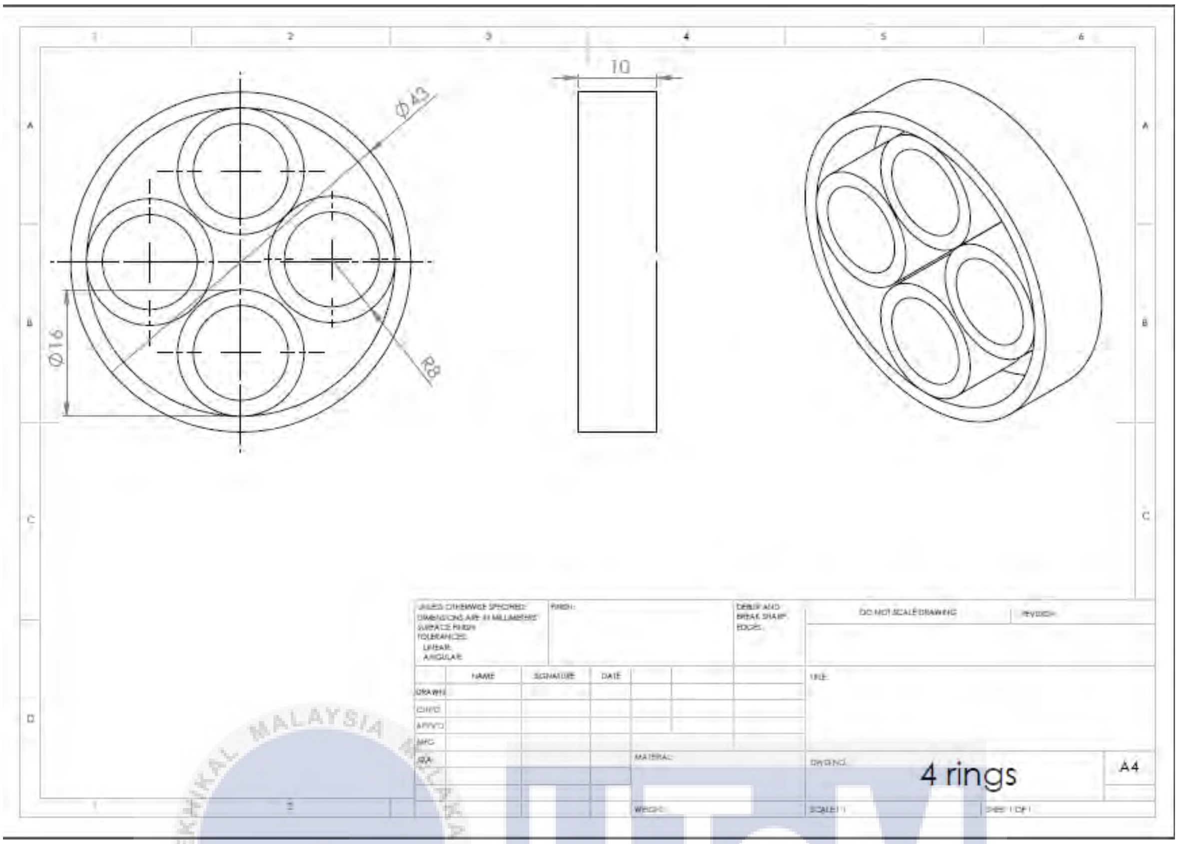

Figure 3.2 Geometry of multi-ring structure

3.3 Tensile testing

3.3.1 Preparation of tensile test specimen

A mild steel circular tube will be used as the material for the multi-ring structure. In order to determine the mechanical properties (yield strength, modulus of elasticity, ultimate tensile strength, maximum displacement) a tensile test has to be conducted. ASTM E8 (Standard Test Methods for Tension Testing of Metallic Materials) standard was referred to determine the mechanical properties through tensile testing.

Figure 3.3 shows the dimension that was referred to draw the tensile test specimen using the AutoCAD software version 2008. These dimensions were used because the material used is a metallic circular tube and the thickness of the wall is below 20mm. Figure 3.4 shows the drawing of the tensile test specimen using AutoCAD which was based on the dimensions provided on Figure 3.3.

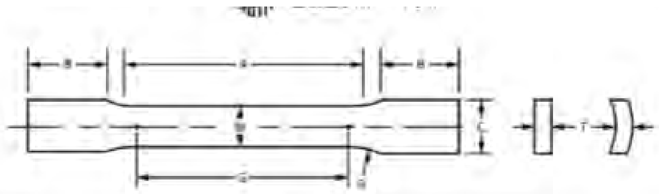

	Dimensions						
	Specimen 1	Specimen 2	Specimen 3	Specimen 4	Specimen 5	Specimen 6	Specimen 7
	mm [in.]	mm [in.]	mm [in.]	mm [in.]	mm [in.]	mm [in.]	mm [in.]
G—Gauge length	50.0 ± 0.1 [2.000 ± 0.005]	50.0 ± 0.1 [2.000 ± 0.005]	200.0 ± 0.2 [8.00 ± 0.01]	50.0 ± 0.1 [2.000 ± 0.005]	100.0 ± 0.1 [4.000 ± 0.005]	50.0 ± 0.1 [2.000 ± 0.005]	100.0 ± 0.1 [4.000 ± 0.005]
W—Width (Note 1)	12.5 ± 0.2 [0.500 ± 0.010]	40.0 ± 2.0 [1.5 ± 0.125-0.25]	40.0 ± 0.2 [1.5 ± 0.125,-0.25]	20.0 ± 0.7 [0.750 ± 0.031]	20.0 ± 0.7 [0.750 ± 0.031]	25.0 ± 1.5 [1.000 ± 0.062]	25.0 ± 1.5 [1.000 ± 0.062]
T—Thickness	measured thickness of specimen						
R—Radius of fillet, min	12.5 [0.5]	25 [1]	25 [1]	25 [1]	25 [1]	25 [1]	25 [1]
A—Length of reduced parallel section, min	60 [2.25]	60 [2.25]	230 [9]	60 [2.25]	120 [4.5]	60 [2.25]	120 [4.5]
B—Length of grip section, min (Note 2)	75 [3]	75 [3]	75 [3]	75 [3]	75 [3]	75 [3]	75 [3]
C—Width of grip section, approximate (Note 3)	20 [0.75]	50 [2]	50 [2]	25 [1]	25 [1]	40 [1.5]	40 [1.5]

Figure 3.3 ASTM E8 Dimensions that could be used in preparing the tensile test specimen for circular tube with thickness below 20mm

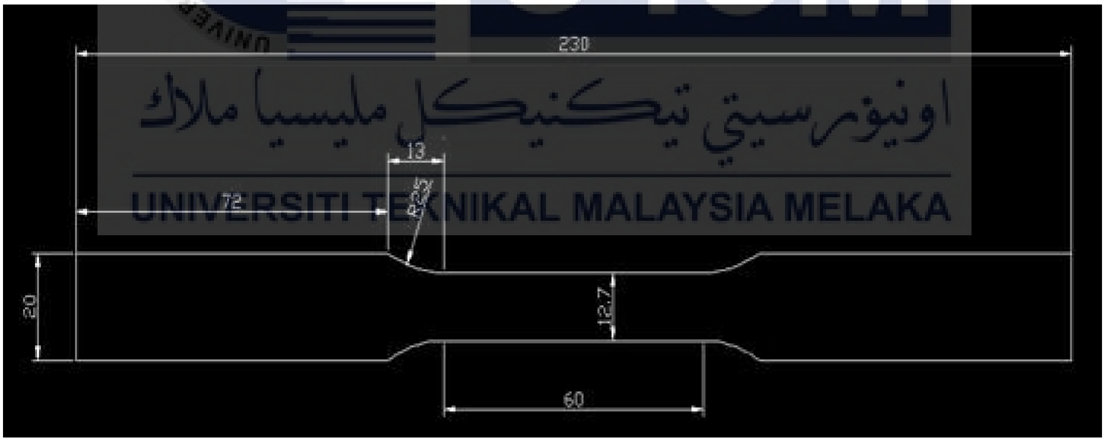

Figure 3.4 AutoCAD drawing of the tensile test specimen (All dimensions are in mm)

Laser cutting machine (as shown in Figure 3.6) from the Faculty of Manufacturing Engineering was then used to cut the tensile test specimen from the mild steel circular tube. Drawing made from the AutoCAD software was transferred to the machine for writing the code. This was done by the technician of the Faculty of Manufacturing Engineering. A total of three specimens was cut from the mild steel circular tube (Figure 3.5) with a length of 600mm. Figure 3.7 shows the tensile test specimen which was cut using the laser cut machine.

Figure 3.5 600mm mild steel circular tube used for laser cutting

Figure 3.6 Laser cutting machine

Figure 3.7 Tensile test specimen

3.3.2 Conducting tensile test

Instron 8872 Universal Testing Machine as shown in Figure 3.8, was used to carry out the tensile test. Before conducting the test, marking was done on all the three specimens, whereby these markings acted as a guide for gripping the tensile test specimen and for placing the extensometer. Extensometer is used to measure the changes in dimension of the tensile test specimen in terms of its length. A 30mm marking was done on both sides of the grip section. Two lines having length of 25mm between one and another was marked on the mid-section of the tensile test specimen for the placement of extensometer.

The tensile test specimen was then gripped onto the gripper of the machine based on the marking done on both sides of the grip section. The reason why this was done is because to make sure that the tensile test specimen is aligned with the machine gripper so that uniaxial loading is parallel to the tensile test specimen. The extensometer was then clipped on the marked position on the tensile test specimen.

Next, the required data such as the thickness, width and length of the tensile test specimen was keyed in. The loading speed was set at 5mm/min and strain increase was set to be at 1%. All readings were reset to be zero to avoid zero error and loading was applied to the tensile test specimen. The extensometer was then removed when it reaches the strain of 1%.

Once the tensile test specimen fractures, results containing stress-strain graph, maximum displacement, yield strength, ultimate tensile strength and modulus of elasticity was printed out. The experiment was then repeated for three times to obtain an average reading.

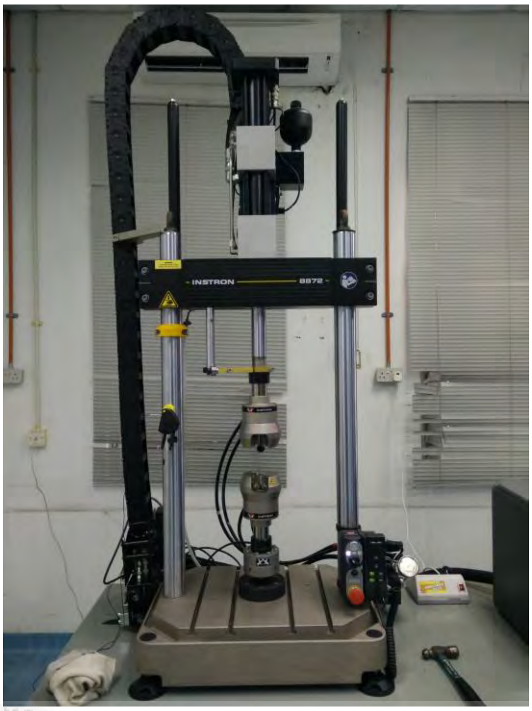

Figure 3.8 Instron 8872 Universal Testing Machine

3.4 Ring specimen fabrication

Two types of rings were prepared for the experimental work which are the single ring and the multi-ring. The rings were cut from a mild steel tube (Figure 3.5) at a width of 10mm using a disc cutter shown in Figure 3.9. Then, the burr on the ring were removed using a file because these burrs could affect the performance of ring as an impact energy absorption device. For the internal ring, it was cut using a tube cutter shown in Figure 3.10 since it has a smaller diameter and it could produce a clean cut without the existence of burr. Metal Inert Gas (MIG) welding method was used to weld the internal rings with the external ring. The rings were welded at each contact point, in-line with the external ring both at the front and back of the ring as shown in Figure 3.11. This is to ensure that the internal ring would not displace in a traverse direction when load is subjected on the ring.

Figure 3.9 Disc cutter machine

Figure 3.10 Tube cutter

Figure 3.11 Welded multi-ring

3.5 Compression test

There were two types of test which were conducted to study the energy absorption capacity of a multi ring which were the quasi-static test and dynamic test. The rings were laterally compressed under quasi-static loading and dynamic loading. Single ring was also laterally compressed in order to compare the energy absorbing capacity with the multi ring. The main difference between these two tests were the loading rate that was subjected to the multi ring.

3.5.1 Quasi-static test

For the quasi-static test, the Instron UTM machine was used to compress the multi ring as well as the single ring. The settings in the computer was set-up by the technician by keying in the relevant details such as the dimension of the rings and the output results that the user needs for analysis purpose. The speed of compression was set with a loading rate of 2mm/min. The ring was placed in the middle of the platen to ensure an equal distribution of load on the ring and also to prolong the machine's life span. At the same time, a Sony 4K Handy-camera was used to record the deformation of the ring when subjected to compression with the aid of two lighting kits as shown in Figure 3.12. The compression test and video recording was started simultaneously and ended as the ring crushes fully. Instructions were given orally every 2mm referring to the computer as loading increases, which would be recorded by the video camera. This is to study the deformation of the rings as load is subjected. The raw data were then collected for analysis purpose which were discussed in Chapter 4 of this report.

Figure 3.12 Quasi-static experimental set up

3.5.2 Dynamic test

The machine used to conduct the dynamic/impact test was the Drop Impact Instron CEAST 9340 machine (Figure 3.17). This machine has a maximum drop weight and a maximum height of stroke of 30kg and 800mm respectively. The machine could be controlled in terms amount of potential energy (mass, and height) and velocity. For this experiment, the potential energy was controlled. Therefore the parameters that were set was the height and mass of drop. This is because potential energy is the product of mass, height and gravity. The amount of potential energy set was estimated to be twice the amount of energy obtained from the quasi-static test. Therefore, from the estimated potential energy, the height and mass was set as shown in Table 4.6 and Table 4.9. Loading subjected on flat plates method were used for this experimental work.

An Olympus i-Speed tr high-speed camera (Figure 3.13) at 1000 frame per second was used to record the motion when the ring was subject to an impact. Lighting plays a crucial part in the recording of the slow-motion video and two lighting kits were used in this experiment as shown in Figure 3.15.

After the camera was set-up, the ring was taped onto a plate to avoid any movement/rotation. Besides, the tape was used to maintain the position of the internal ring, whereby the upper and lower internal ring is parallel in position as shown in Figure 3.16. As the height and mass was set in the computer, the drop test begins simultaneously with the slow-motion video recording. After crushing the ring, the video was edited using the control display unit as shown in Figure 3.14. The raw data was collected and later discussed in the following chapter.

Figure 3.13 Olympus i-speed tr camera

Figure 3.14 Control display unit

Figure 3.15 Lighting kits

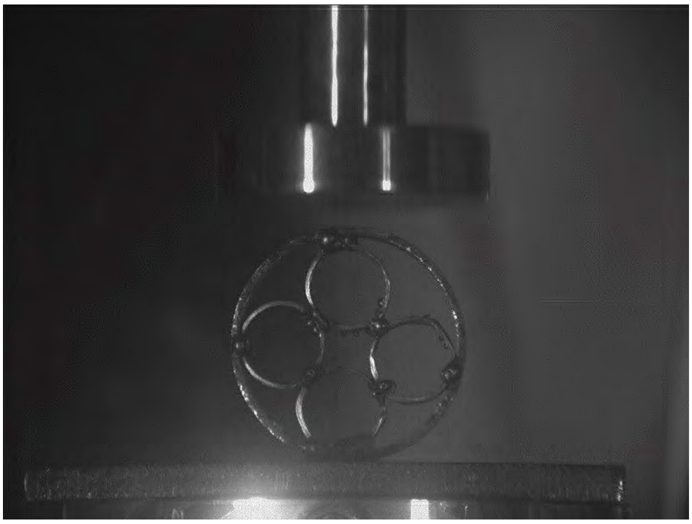

Figure 3.16 Position of multi-ring (Bottom internal ring perpendicular to the platen)

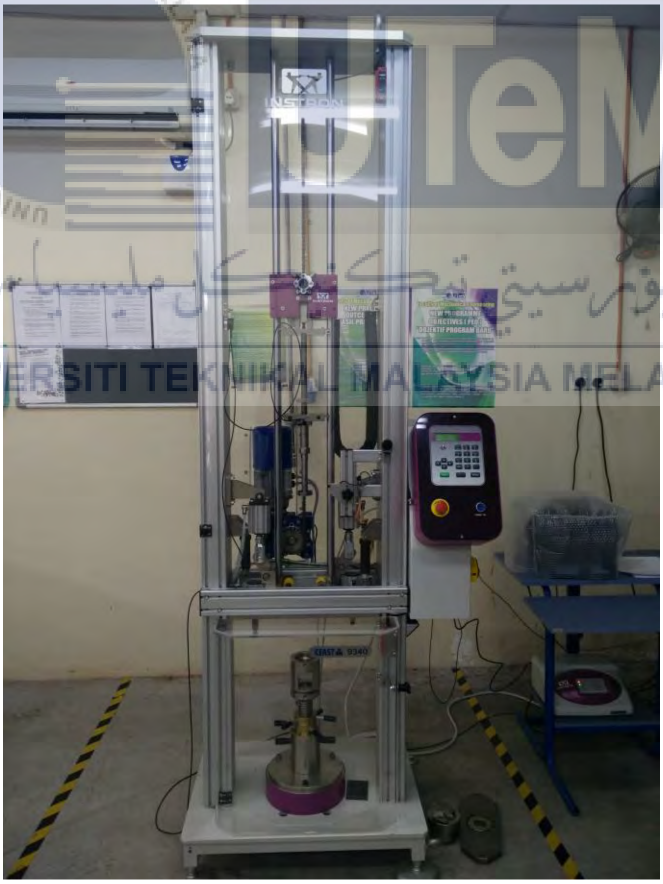

Figure 3.17 Drop Impact Instron CEAST 9340 machine

CHAPTER 4

RESULT AND DISCUSSION

4.1 Tensile Test

Tensile test was conducted using the Instron 8872 Universal Testing Machine to obtain the mechanical properties of mild steel circular tube. Mechanical properties such as the yield strength, Young's modulus, ultimate tensile strength and maximum displacement made by the material when subjected to tensile loading was obtained from the tensile test. These mechanical properties are crucial in an energy absorbing device and will be used for further calculations of this project.

Table 4.1 shows the results obtained from the tensile test conducted on the mild steel material. Besides that, stress-strain graph was also drawn for each test specimen as shown from Figure 4.2 to Figure 4.4. A total of three tensile test specimen were tested to obtain an average and accurate reading of the mechanical properties of the mild steel circular tube. Although three specimens were tested, data from specimen 3 had properties that were very much close with the ones provided by in the table of typical properties of selected materials used in engineering. The difference caused by the other two specimens maybe due to the rust surface of the mild steel material. Therefore data from specimen 3 was used throughout the analysis.

Figure 4.1 shows the conditions of the tensile test specimen after fracture. Based on the observation made, all three specimens showed properties of a ductile material since all has fracture surface of approximately 45 ° to the direction of tensile loading. On the other hand, the graph of stress-strain plotted indicates that the mild steel has high strength, high toughness and high ductility.

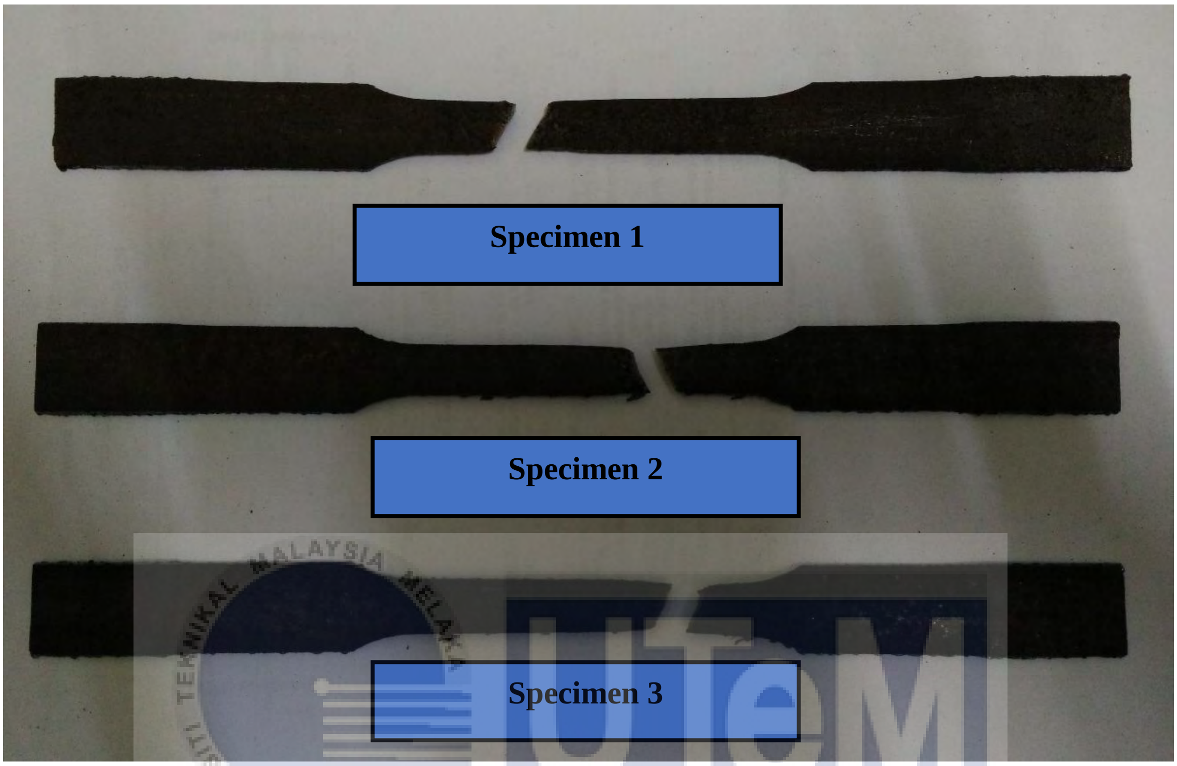

Figure 4.1 Tensile test specimens after fracture

Table 4.1 Results of mechanical properties for circular mild steel tube

Mechanical properties	**Tensile test specimen 1**	**Tensile test specimen 2**	**Tensile test specimen 3**
Maximum load(kN)	7.428	7.184	7.531
Tensile stress at Maximum load (MPa)	382.114	331.231	387.393
Tensile stress at yield(MPa)	360.653	313.015	361.322
Load at break (kN)	1.793	4.174	4.0222
Tensile stress at break (MPa)	92.257	192.450	206.883
Tensile extension at break (mm)	9.127	8.983	8.292
Tensile strain at break (mm/mm)	0.365	0.359	0.332
Young's modulus (MPa)	148.887	157.143	184.063

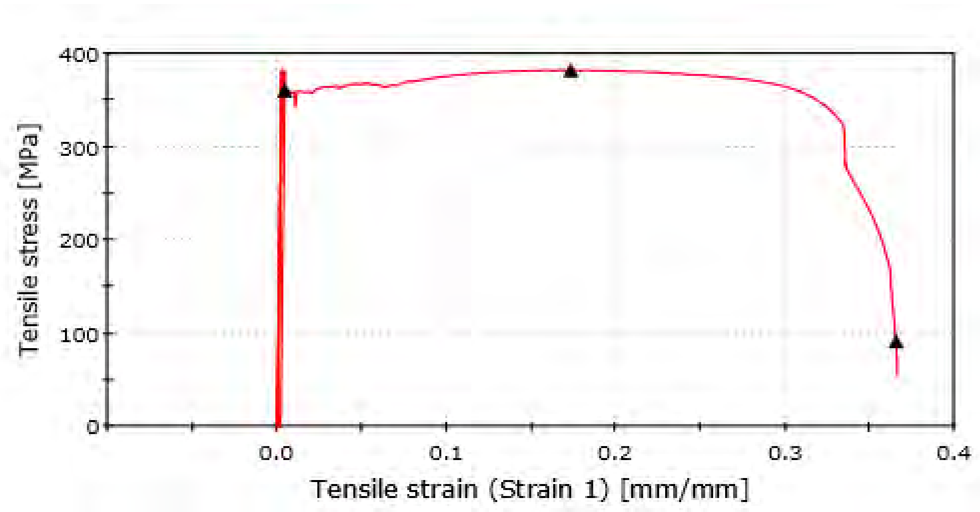

Figure 4.2 Stress-strain graph for tensile test specimen 1

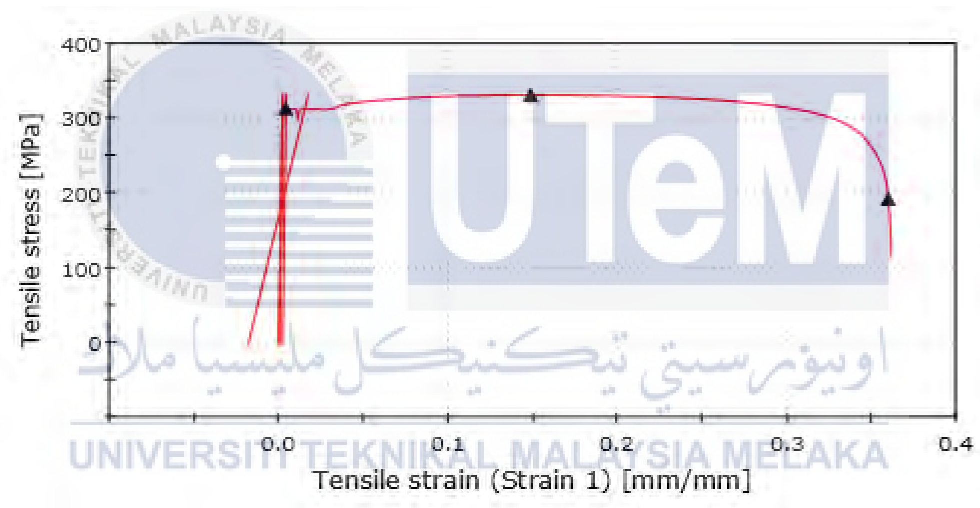

Figure 4.3 Stress-strain graph for tensile test specimen 2

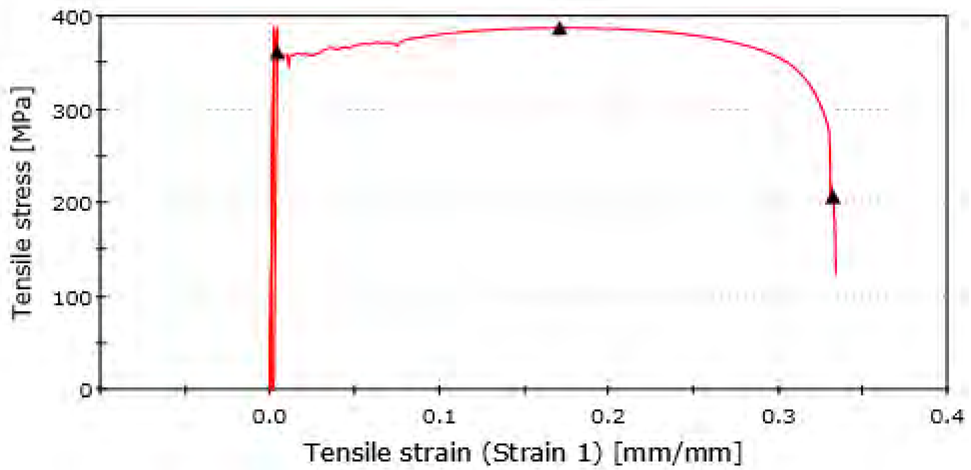

Figure 4.4 Stress-strain graph for tensile test specimen 3

4.2 Compression test

Results from the quasi-static test and dynamic test were discussed in this chapter. To prove that the multi ring has a higher energy absorption capacity, comparisons were done in terms of experimental work between multi ring and singular ring.

4.2.1 Quasi static loading

Quasi static loading test was conducted on both the single ring and multi ring in order to determine the energy absorbing capacity of both the types of rings. Theoretical calculations were also made using the respective mathematical formulas to determine the collapse load, P_0 and were compared with the experimental values. Experimental value for collapse load was obtained from the graphs drawn (Figure 4.5 to Figure 4.7), which was taken from the first peak of those respective graphs.

Single ring

A total of 3 specimens were quasi-statically loaded for the singular ring. Table 4.2 shows the comparison of collapse load between theoretical and experimental for single ring under quasi-static loading. The formula used and the ring geometry is shown below. From the comparisons made, there is an average percentage of 40% difference between the theoretical and experimental value of collapse load.

Using methods similar with ring compressed by flat plates, collapse load is,

$$P_0 = \frac{4M_0}{R} = \frac{\frac{4\sigma_0 t^2}{4}}{R} = \frac{\sigma_0 t^2}{R}$$

Yield strength, σ_0 = 361.322 MPa

Thickness, t = 2mm

Outer diameter, D = 42.3mm

Radius, R = 21.15 mm

Width = 10 mm

$$P_0 = \frac{(361.322\ x\ 10^6)(0.002)^2}{0.02115}$$

$= 68335.13$ N/m

$= 68335.13 \times (10 \times 10^{-3})$

$= 683.35$ N

Table 4.2 Theoretical and experimental collapse load for single ring under quasi-static loading

	Collapse Load, P_0 (N/m)		Percentage error,
	Theoretical	Experimental	(%)
Sample 1	683.35	422.7270	38.13
Sample 2	683.35	377.1595	44.81
Sample 3	683.35	420.3644	38.48

Raw data obtained from the Instron machine was used to plot the graph of load versus displacement as shown below from Figure 4.5 to Figure 4.7. The load versus displacement graphs for singular ring shown from Figure 4.5 to Figure 4.7 were plotted until the plateau zone (beginning of densification zone) at displacement 28.242mm. The useful energy absorbed by the rings (inclusive of single ring and multi-ring) is obtained from area under the graph of load versus displacement until the plateau zone. The area at densification zone is not taken since the energy absorbed at that zone is not by the ring structure, but by the mild steel material itself. Therefore, the beginning of densification zone for single rings under quasi-static loading is assumed to be at a displacement of 28.242mm. The method of obtaining the densification at a certain displacement is shown at Figure 4.9 in detail. For all the singular rings which were quasi-statically loaded, the force and displacement increases linearly until it reaches the collapse load point at approximately 400N. After the point of collapse load, the ring starts to deform from a displacement of approximately 2mm. Force is then continued to be exerted up to 70% to 80% of the ring diameter to avoid self-contact of the ring. Table 4.3 shows the useful energy absorbed by three single ring specimens. The average energy absorption capacity for a single ring is 14181.47 Nmm or 14.18 J.

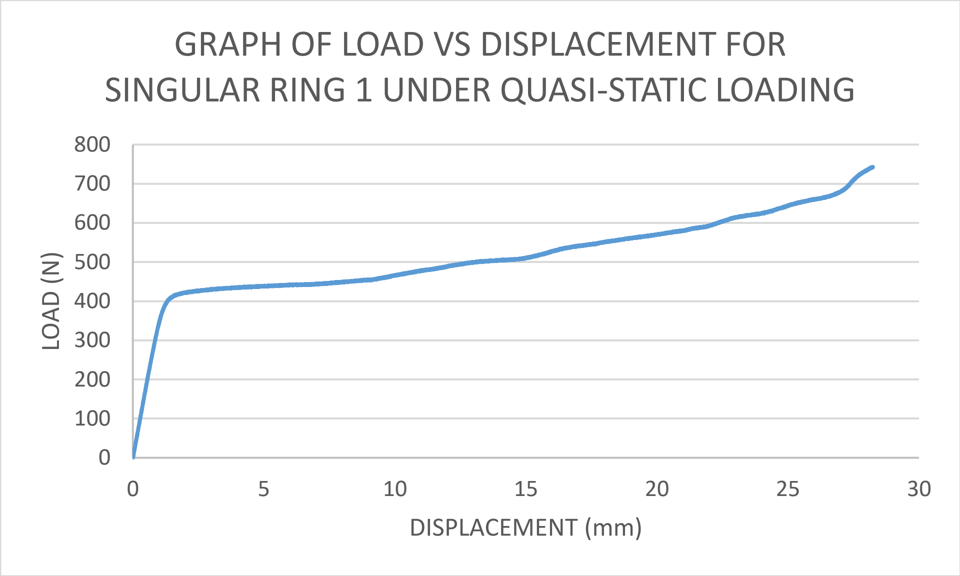

Figure 4.5 Graph of load versus displacement for singular ring 1 under quasi-static loading

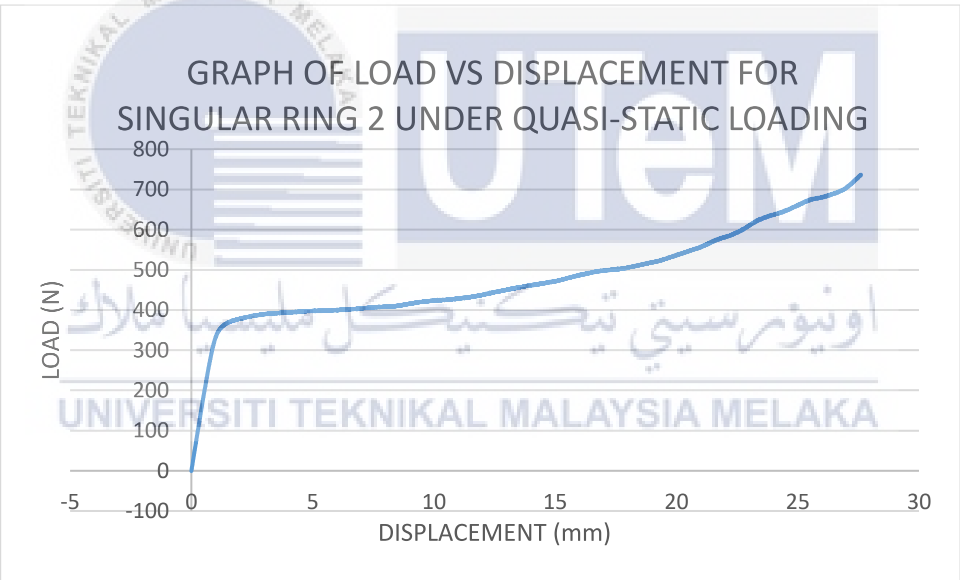

Figure 4.6 Graph of load versus displacement for singular ring 2 under quasi-static loading

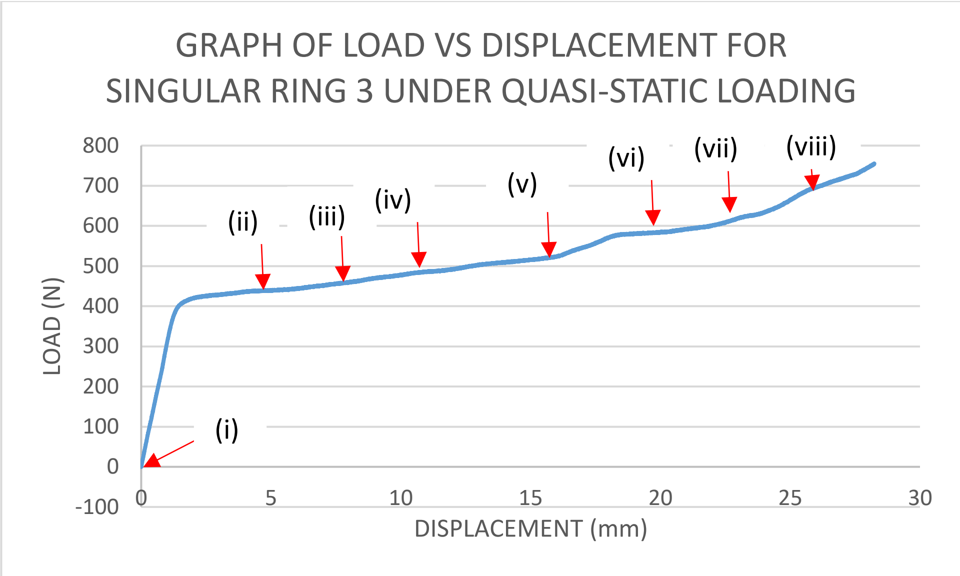

Figure 4.7 Graph of load versus displacement for singular ring 3 under quasi-static loading

Table 4.3 Energy absorbed by single ring under quasi static loading

Useful energy absorbed /	Area under the graph until plateau zone
Sample 1	14520.88 Nmm
Sample 2	13272.98 Nmm
Sample 3	14750.56 Nmm
Average energy absorbed	*14181.47 Nmm*

The deformations of single ring under quasi-static loading is shown below at Figure 4.8. Figure 4.8 shows the deformation of single ring under quasi-static loading referring its point of deformation with Figure 4.7.

(i)δ = 0mm (ii)δ = 4mm

(iii)δ = 8mm (iv)δ = 12mm

(v)δ = 16mm (vi)δ = 20mm

(vii)δ = 24mm

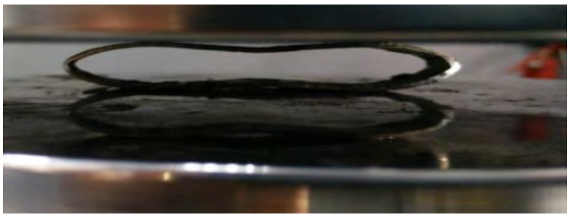

(viii)δ = 28mm

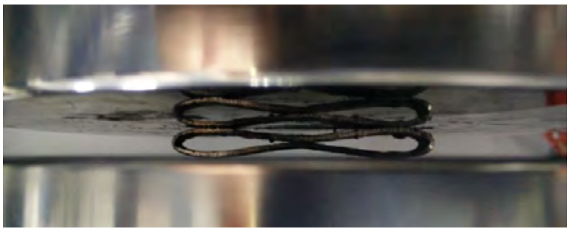

(ix)δ = 34mm

Figure 4.8 Deformations of single ring structure at various displacements under quasi-static loading

Multi ring

A total of 4 multi ring specimens were quasi-statically loaded with a loading rate of 2mm/min using the Instron UTM machine. Comparison between theoretical and experimental values were done for the collapse load, P_0 of multi ring structure as shown in Table 4.4. Experimental collapse load value were taken from the first peak of the load versus displacement graph plotted as shown from Figure 4.9 to Figure 4.12. For the theoretical calculation, methods of ring compressed by two flat plate and rings constrained by a V-block under flat plate compression were used. Mathematical formula and geometries of rings is shown as below:

i) External ring is assumed to be compressed by two flat plate method. Therefore, collapse load,

$$P_0 = \frac{\sigma_0 t^2}{R}$$

ii) Internal rings are assumed to be constrained by a V-block under flat plate compression. Therefore collapse load,

$$P_0 = \frac{4\,M_0 \cot[(\pi+\alpha)]/8}{R}$$

$$= \frac{\sigma_0 t^2 \cot[(\pi+\alpha)]/8}{R}$$

Dimensions and properties of external ring

Yield strength, σ_0 = 361.322 MPa

Thickness, t = 2mm

Outer diameter, D = 42.3mm

Radius, R = 21.15 mm

Width = 10 mm

Dimensions and properties of internal ring

Yield strength, σ_0 = 361.322 MPa

Thickness, t = 2mm

Outer diameter, D = 15.9mm

Radius, R = 7.95 mm

Width = 10 mm

Sample calculation of collapse load, P_0 for external ring and four internal rings.

P_0 (external) = 68335N (P_0 is similar with singular ring)

Collapse load for 1 ring, P_0 (internal) $= \dfrac{(361.322\ x\ 10^6)(0.002)^2 \cot[(\pi + 60°)]/8}{0.00795}$

= 7042.8248 N/m

= 7042.8248 x (10 x 10^{-3})

= 70.43 N

Total collapse load $\Sigma P_0 = P_0$ (external) + P_0 (internal)

$$= 683.35 + (4 \times 70.43)$$

$$= 965.0713\text{N}$$

Table 4.4 Theoretical and experimental collapse load for multi ring under quasi-static loading

	Collapse Load, P_0 (N/m)		Percentage error, (%)
	Theoretical	Experimental	
Sample 1	965.0713	762.4066	22.04
Sample 2	965.0713	969.1332	0.42
Sample 3	965.0713	1063.4168	9.25
Sample 4	965.0713	928.4313	3.80

From Table 4.4, it shows that the multi ring has an average of 8% of percentage error between the theoretical and experimental value of collapse load. Figure 4.9 to Figure 4.12 shows the graph of load versus displacement for all 4 multi ring specimens. Methods on how the densification zone at a particular displacement is shown in Figure 4.9.

The figure below (Figure 4.9) shows the method on how the densification zone of a ring (this method was used for both multi ring and single ring). A linear line (grey in colour) was plotted along the collapse load point and then a linear equation was obtained from that line. Using the slope value of that line which is 629.06*x*, a parallel line (yellow in colour) was plotted at the right end of the graph making sure it touches the parabolic curve from the load versus displacement graph. Then, a linear line (black in colour) was projected from the point of collapse load until it intersects with the yellow line. The intersection between the yellow line and the black line indicates the displacement at which the densification zone starts. The displacement at densification zone for multi ring is at 26.2958mm.

There are three regions in a typical load-displacement curve, which are the linear region, plateau region and densification region. In the first region, the response is linear elastic followed by the plateau region where initial collapse load is reached and a large amount of deformation could be seen in this region. Then, the load increases rapidly as a result of compaction/compression of the mild steel material. The useful energy of an impact energy absorber is determined until the transition point of plateau zone to densification zone. Therefore, all graphs shown in this report were plotted until the plateau zone only.

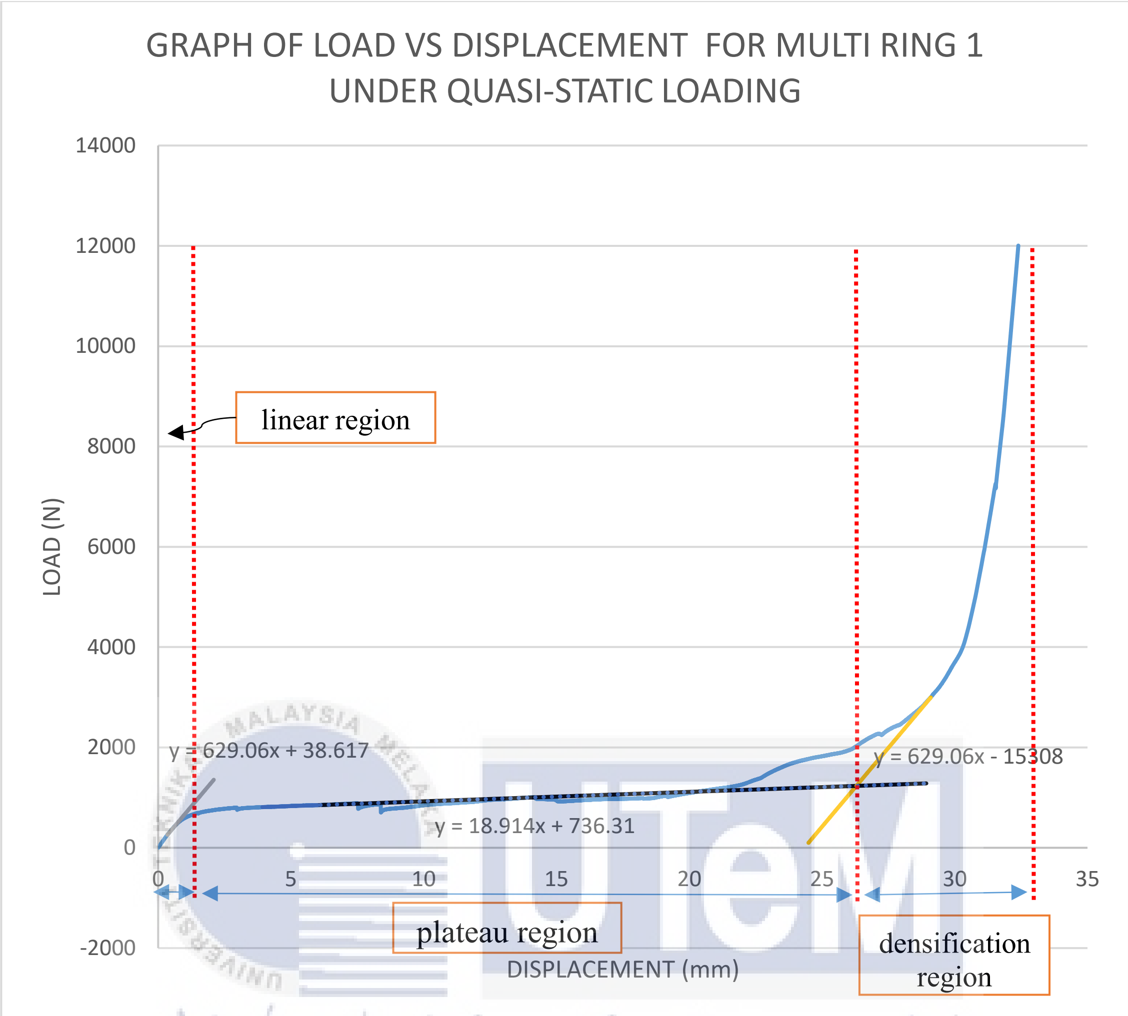

Figure 4.9 Graph of load versus displacement for multi ring 1 under quasi static loading

Graphs shown from Figure 4.9 to Figure 4.12 is the graph of load versus displacement for the multi ring specimens under quasi static loading. The graphs were plotted until the plateau zone which is at a displacement of 26.2958mm. Value of area under the graph which is tabulated in Table 4.5 shows the useful energy absorbed by the multi ring structure having an average energy absorption capacity of 31018.25 Nmm or 31.02 J. The force exerted on the multi ring increases linearly with the displacement until it reaches its collapse zone at an approximate load of 950N. Then, significant amount of deformation could be seen starting from 2mm. The sudden fluctuations in the graphs indicate that the surface of the ring was crushing on the welded burr which was formed during the welding process. These fluctuations are not good for an impact energy absorbing device because it could give an effect to the energy absorbing capacity of the multi ring structure. To have a good energy absorbing capacity, the load and displacement curve should be in a smooth incremental manner. Since welding method is highly dependent on the skills of the welder, this problems sometimes could not be avoided unless a different method is used to join the internal mild steel rings with the external mild steel ring. As deformation of the multi ring increases, the moment arm becomes shorter which requires greater force to maintain the deformation of the ring. This is the reason behind why the force increases rapidly after the plateau zone as shown in Figure 4.9.

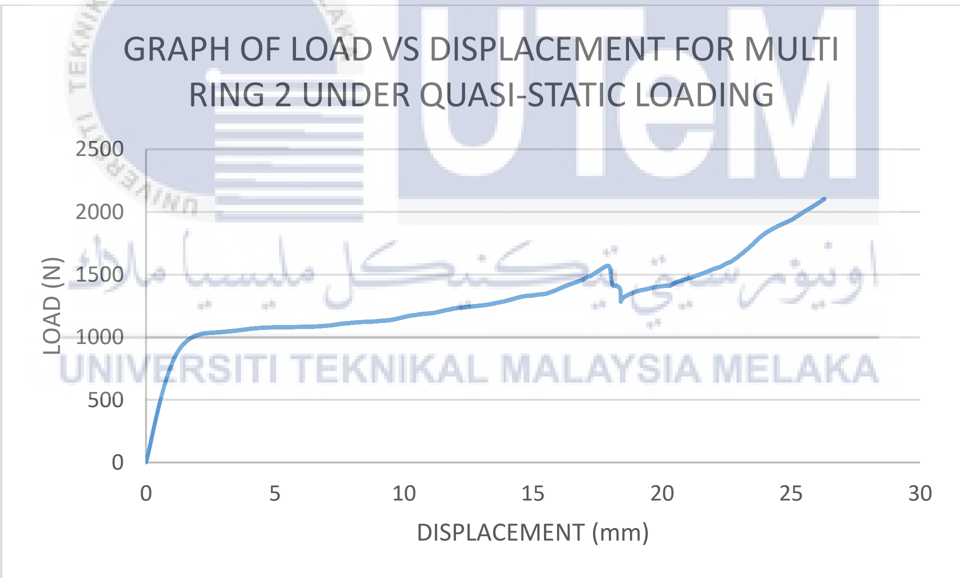

Figure 4.10 Graph of load versus displacement for multi ring 2 under quasi static loading

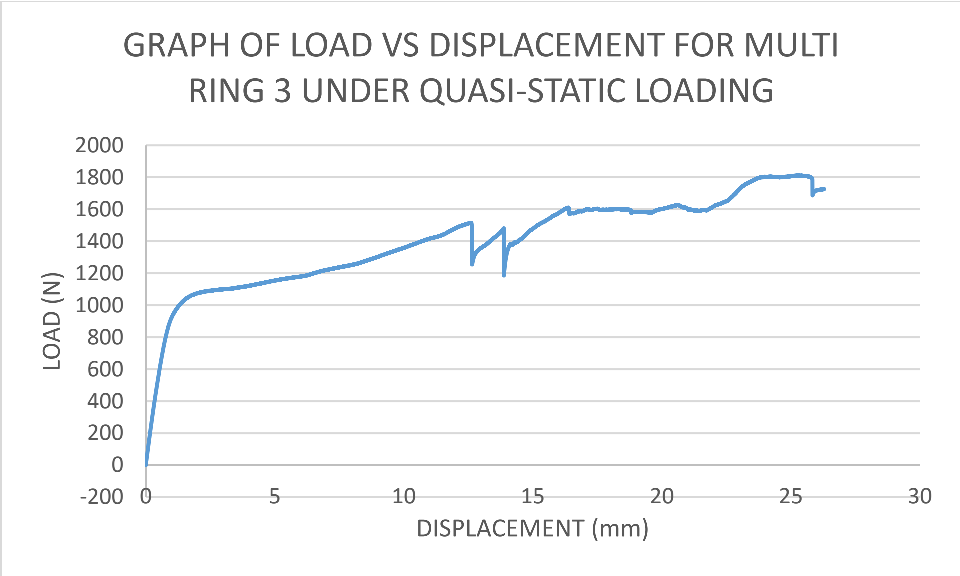

Figure 4.11 Graph of load versus displacement for multi ring 3 under quasi static loading

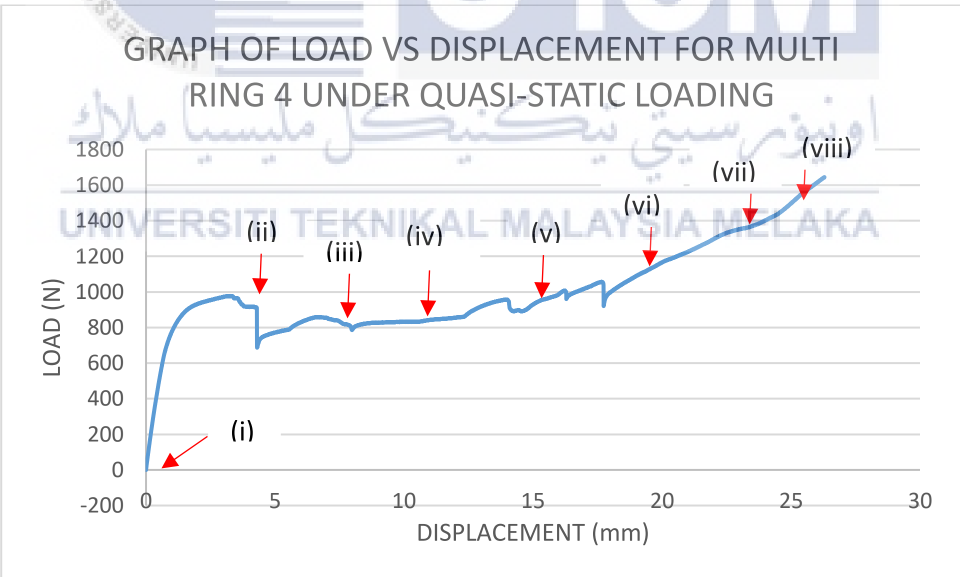

Figure 4.12 Graph of load versus displacement for multi ring 4 under quasi static loading

Table 4.5 Energy absorbed by multi ring under quasi static loading

Useful energy absorbed /	**Area under the graph until plateau zone**
Sample 1	26745.9 Nmm
Sample 2	34117.07 Nmm
Sample 3	36834.6 Nmm
Sample 4	26375.41 Nmm
Average energy absorbed	*31018.25 Nmm*

Figure 4.13 shows the deformation images of the multi ring from 0mm to 28mm at an interval of 4mm. It shows the deformation of single ring under quasi-static loading referring its point of deformation with Figure 4.12.

(i)δ = 0mm

(ii)δ = 4mm

(iii)δ = 8mm (iv)δ = 12mm

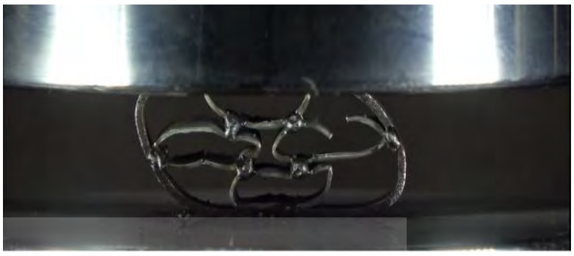

(v)δ = 16 mm (vi)δ = 20 mm

(vii)δ = 24 mm (viii)δ = 26 mm

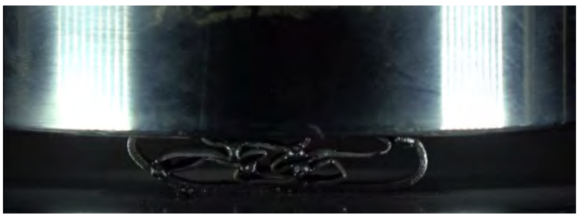

(ix)δ = 28 mm

Figure 4.13 Deformations of multi ring at various displacements under quasi-static loading

Figure 4.14 shows the superimposed graph of singular ring and multi ring under quasi-static loading. From the graph plotted it could be clearly seen that the area under the graph and collapse load for multi ring is higher compared to singular ring. The multi ring structure has a collapse load which is 56% higher compared to multi ring. The same applies for the amount of useful energy absorbed (area under graph until plateau zone), whereby the multi ring structure has an energy absorbing capacity 54% higher than the singular ring. It is proven experimentally that the multi ring has an advantage over the singular since it has a higher energy absorbing capacity and a higher value of collapse load.

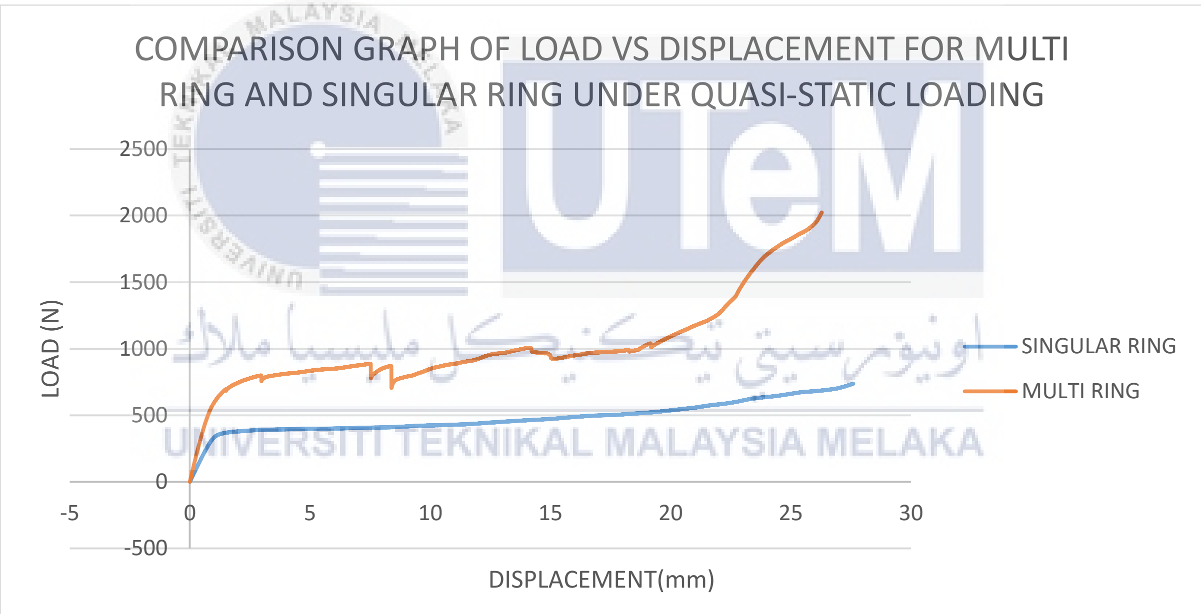

Figure 4.14 Graph of comparison between multi ring and singular ring

4.2.2 Dynamic loading

Although, it was already proven that the multi ring has a higher energy absorption capacity than the single ring in the quasi-static loading test, dynamic loading was conducted on both the types of rings. This is to study the effect of strain rate on the ring structures since impact energy absorption devices are devices which may subject to dynamic loading or sudden impact. When there is a dynamic load subjected on the ring, there will be a sudden increase on the yield stress of the material itself. Therefore, dynamic yield stress has to be used in order to calculate the collapse load of the ring structures. Shown below are the formula used to obtain the dynamic yield stress, strain rate and velocity of the stroke:

$$\frac{\sigma_{0d}}{\sigma_0} = 1 + \left(\frac{\dot{\varepsilon}}{B}\right)^{1/q}$$

$$\dot{\varepsilon} = \frac{V}{2R}$$

$$V = \sqrt{2gh}$$

Based on Copper-Symonds relation, parameters for representative rate-sensitive mild steel material is:

B (s^{-1}) = 40

q = 5

Although the common material constant B and q used in the Copper-Symonds relation is 40 and 5, these constants could only be applied on applications with very small strain percentage (0.05). It also appears that the dynamic yield stress was very large if the Copper-Symonds material constant were used. Therefore, based on research conducted by (Olabi et al., 2006) value for the constant B and q are 6844 and 3.91 respectively. These were the constants used for the calculation of dynamic yield stress in this research project.

<u>*Single Ring*</u>

A total of six singular mild steel rings were dynamically loaded with each ring having different drop mass and height of stroke. The variations of mass and height used for the impact test are tabulated as shown in Table 4.6. Table 4.6 shows the Initial velocity, V_0 , Dynamic yield stress, σ_{0d} ,Theoretical collapse load, P_0 Experimental collapse load, P_0 and Percentage difference between theoretical and experimental collapse load. Shown below are the geometries and properties of the single ring and the sample calculation for specimen sample 1 of the single ring.

Thickness, t = 2mm

Outer diameter, D = 42.3mm

Radius, R = 21.15 mm

Width = 10 mm

<u>Sample 1 (Mass = 11.254kg, Height = 270mm)</u>

Initial velocity, $V = \sqrt{2(9.81)(0.27)}$

$= 2.3016$ m/s

Strain rate, $\dot{\varepsilon} = \dfrac{2.3016}{2(21.15 \ x \ 10^{-3})}$

$= 54.4113 \ s^{-1}$

$$\frac{\sigma_{0d}}{\sigma_0} = 1 + (\frac{\dot{\varepsilon}}{B})^{1/q}$$

Dynamic yield stress, σ_{0d} $= \sigma_0 \left[1 + (\frac{\dot{\varepsilon}}{B})^{1/q}\right]$

$= (361.322 \times 10^6) \left[1 + (\frac{54.4113}{6844})^{1/3.91}\right]$

$= 466.2538$ MPa

Collapse load, $P_0 = \frac{\sigma_0 t^2}{R}$

$= \frac{(466.2538 \times 10^6)(0.002)^2}{21.15 \times 10^{-3}}$

$= 88180.38$ N/m

$= (88180.38) \times (10 \times 10^{-3})$

$= 881.8038$ N

Table 4.6 Experimental data and results for singular ring under dynamic loading

Sample	**Mass (kg)**	**Height/ Stroke (mm)**	**Potential energy (J)**	**Initial velocity, V_0 (m/s)**	**Dynamic yield stress, σ_{0d} (MPa)**	**Theoretical collapse load, P_0 (N)**	**Experimental collapse load, P_0 (N)**	**Percentage difference between theoretical and experimental collapse load (%)**
1	11.254	270	29.81	2.3016	466.25	881.80	661.61	25
2	11.254	270	29.81	2.3016	466.25	881.80	656.58	25.5
3	9.254	275	24.96	2.3228	466.50	882.27	675.48	23.4
4	7.254	280	19.93	2.3438	466.74	882.73	791.41	10.3
5	8.254	330	26.72	2.5445	468.98	886.96	534.87	39.7
6	8.254	275	22.27	2.3228	466.50	882.27	666.17	24.5

The experimental collapse load value is taken from the first peak of the graph (as shown in Figure 4.15 to Figure 4.20) before a significant/rapid change of displacement. The average percentage error of collapse load between the theoretical and experimental for single ring is 24%. The average collapse load for singular ring under dynamic loading is 664N and there is a percentage difference of 39% compared to the collapse load of single ring under quasi-static loading. This is mainly because of the effect of strain rate or velocity per unit length subjected on the ring. The effect of strain rate could only be seen in dynamic loading and not in quasi-static loading since the loading rate (2mm/min) is very low and no significant strain rate effect could be seen.

The graphs shown from Figure 4.15 to Figure4.20 are the graphs of load versus displacement for singular ring under dynamic loading and it is plotted until the starting point of densification zone at displacement 28.242mm. Area under the graph shows the useful energy that could be absorbed by the singular ring under dynamic loading. The useful energy absorbed by the ring is tabulated in Table 4.7.

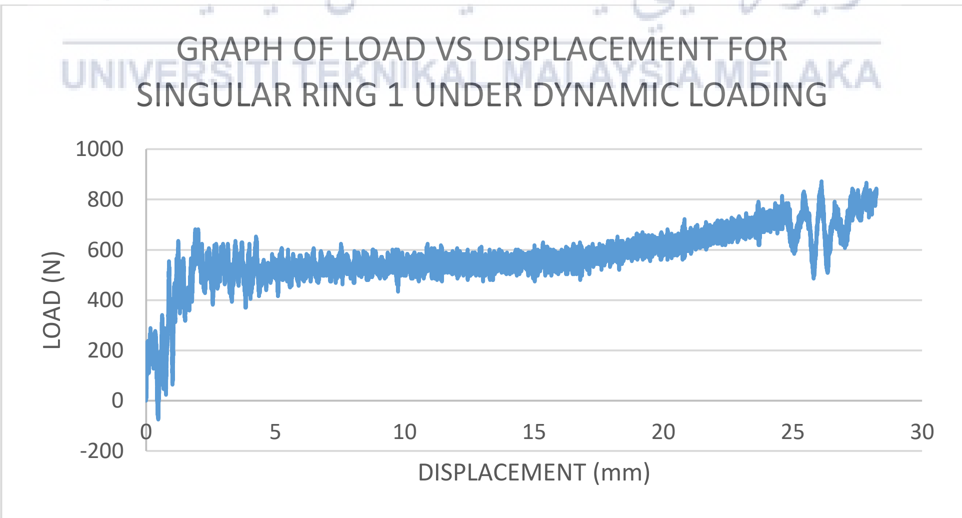

Figure 4.15 Graph of load vs displacement for singular ring 1 under dynamic loading

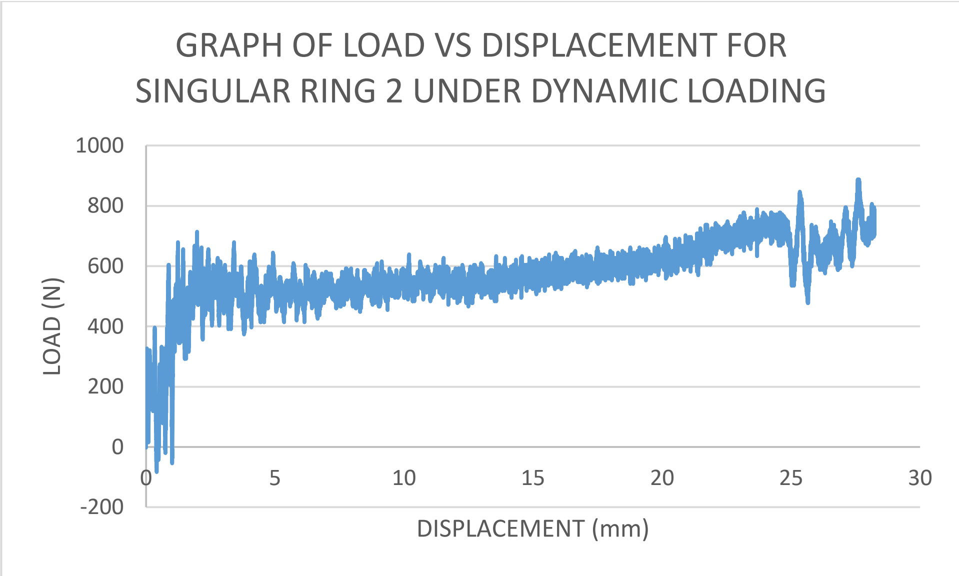

Figure 4.16 Graph of load vs displacement for singular ring 2 under dynamic loading

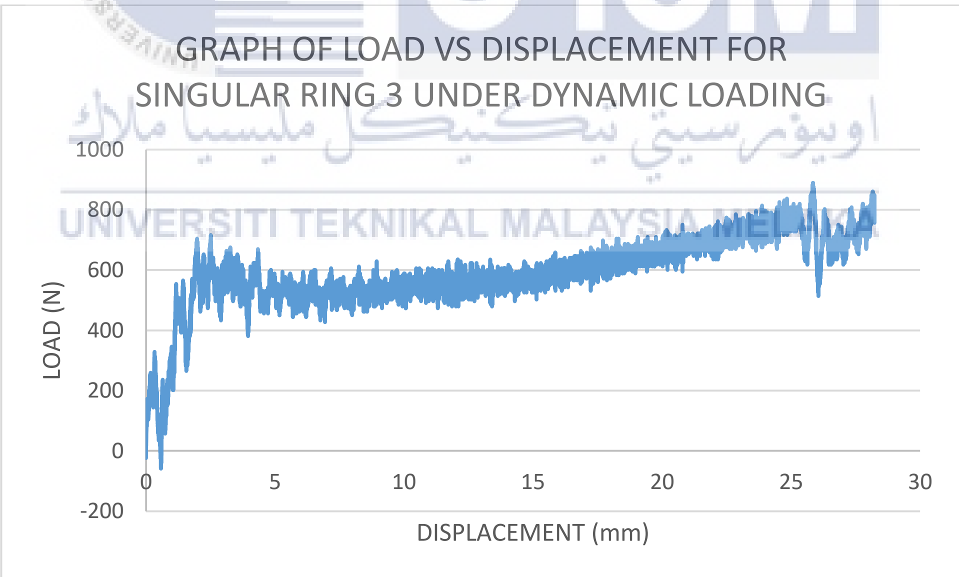

Figure 4.17 Graph of load vs displacement for singular ring 3 under dynamic loading

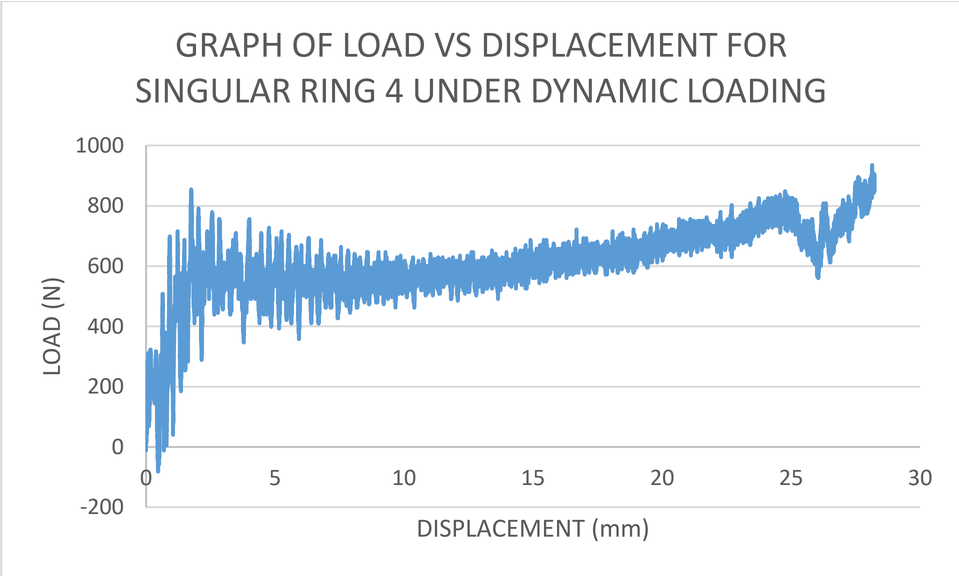

Figure 4.18 Graph of load vs displacement for singular ring 4 under dynamic loading

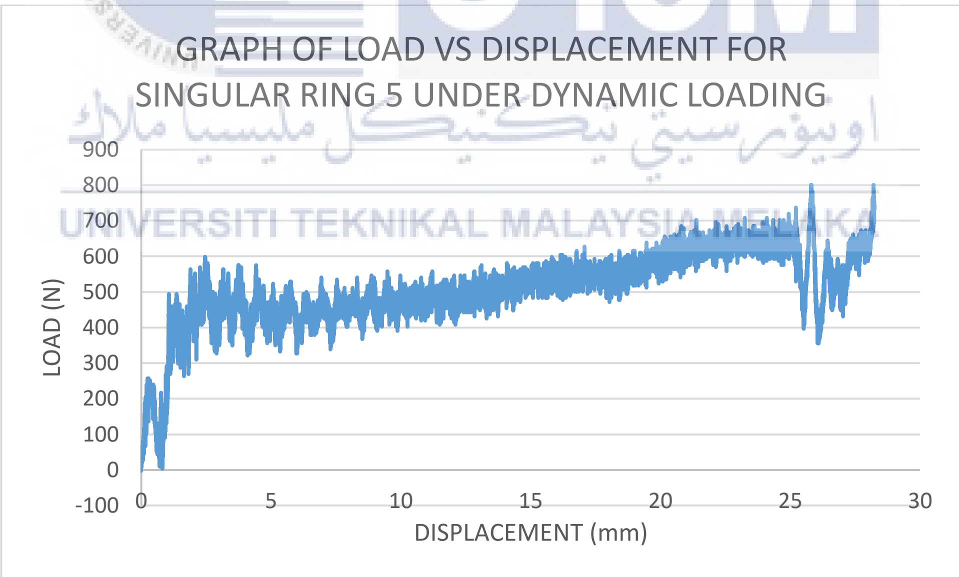

Figure 4.19 Graph of load vs displacement for singular ring 5 under dynamic loading

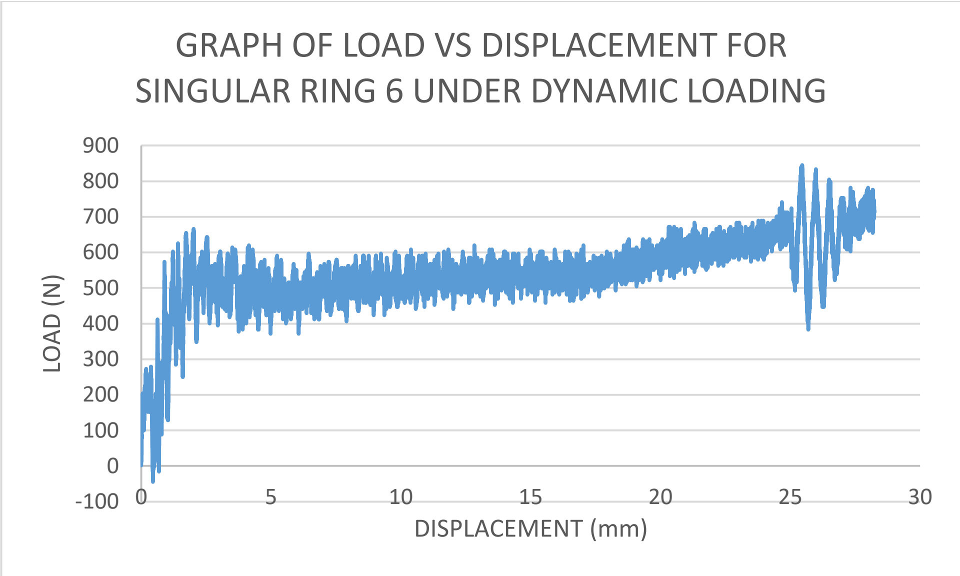

Figure 4.20 Graph of load vs displacement for singular ring 6 under dynamic loading

Table 4.7 Energy absorbed by single ring under dynamic loading

Useful energy absorbed /	**Area under the graph until plateau zone**
Sample 1	16200.79 Nmm
Sample 2	16218.12 Nmm
Sample 3	16702.51 Nmm
Sample 4	17253.58 Nmm
Sample 5	14336.38 Nmm
Sample 6	15322.07 Nmm
Average energy absorbed	*16005.58 Nmm*

The average energy absorbed by the single ring under dynamic loading is 16005.58Nmm or 16 J. Table 4.8 shows the deformed shape shapes of singular ring when it is subjected to impact loading with various mass and height of stroke in a chronological order. From the images shown, it shows that, the higher the amount of potential energy (product of mass, height and gravity) dissipated, the larger the deformation of the ring after impact.

Table 4.8 Chronological order of singular rings samples in terms of amount of potential energy dissipated and in terms of deformation when subjected to dynamic loading.

	Sample	Potential energy (J)
1	 Sample 1	29.81
2	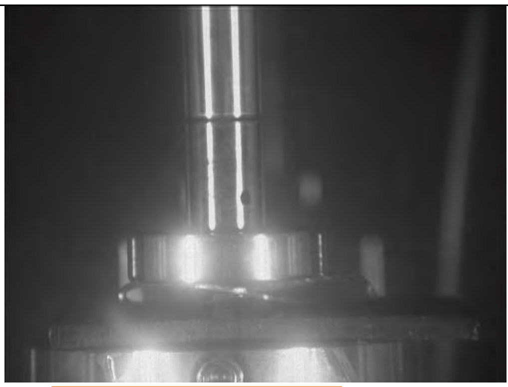 Sample 2	29.81

3	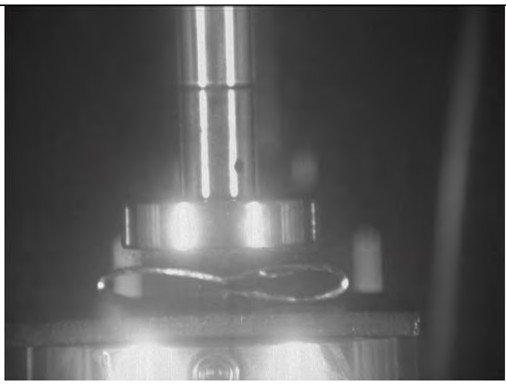 Sample 5	26.72
4	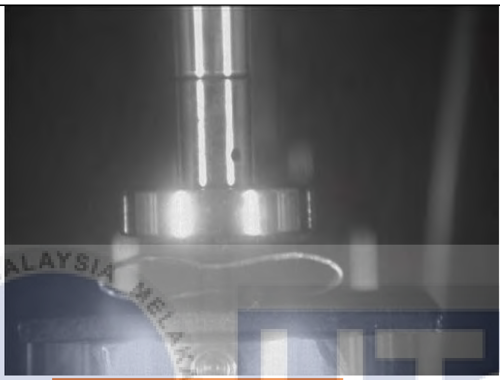 Sample 3	24.96
5	 Sample 6	22.27
6	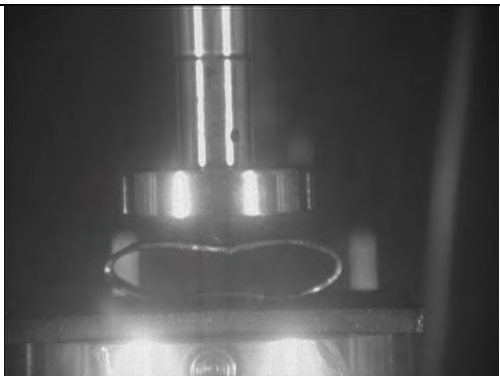 Sample 4	19.90

Figure 4.21 shows the images of single ring subjected to impact which it was recorded in a high-speed camera with each image displaying the frame recorded and time of contact in milliseconds.

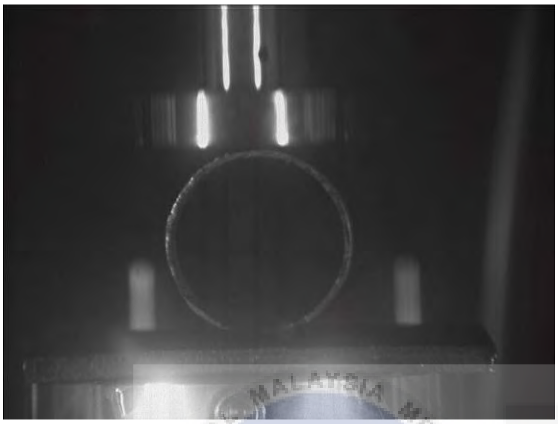

Frame 4:0ms

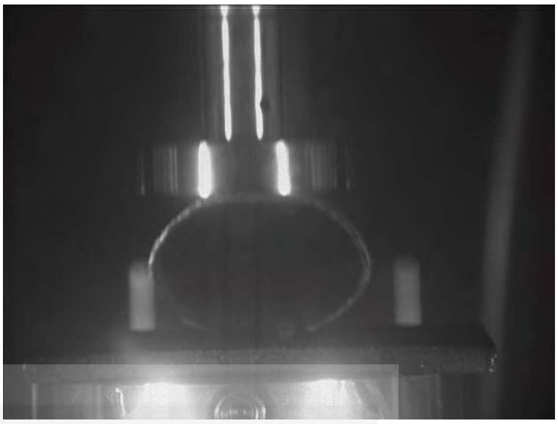

Frame 9:5ms

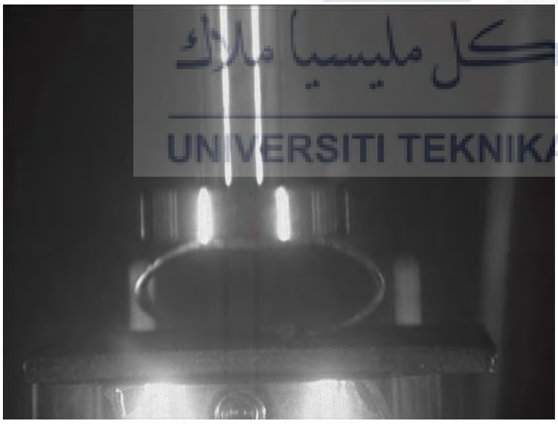

Frame 14:10ms

Frame 19:15ms

Figure 4.21 Displacement of single ring under dynamic loading

Multi ring

A total of 6 multi ring specimens were dynamically loaded with each ring having different drop mass and height of stroke. The variations of mass and height used for the impact test are tabulated as shown in Table 4.9. Table 4.9 shows the Initial velocity, V_0, Dynamic yield stress, σ_{0d} ,Theoretical collapse load, P_0 ,Experimental collapse load, P_0 Percentage difference between theoretical and experimental collapse load. For the theoretical calculation, methods of ring compressed by two flat plate and rings constrained by a V-block under flat plate compression was used. Shown below is the sample calculation for specimen sample 1 of the multi ring as well as the Mathematical formula and geometries of rings:

i) External ring is assumed to be compressed by two flat plate method. Therefore, collapse load,

$$P_0 = \frac{\sigma_0 t^2}{R}$$

ii) Internal rings are assumed to be constrained by a V-block under flat plate compression. Therefore collapse load,

$$P_0 = \frac{4\, M_0 \cot[(\pi+\alpha)]/8}{R}$$

$$= \frac{\sigma_0 t^2 \cot[(\pi+\alpha)]/8}{R}$$

$$\frac{\sigma_{0d}}{\sigma_0} = 1 + (\frac{\dot{\varepsilon}}{B})^{1/q}$$

$$\dot{\varepsilon} = \frac{V}{2R}$$

$V = \sqrt{2gh}$

Based on Copper-Symonds relation, parameters for representative rate-sensitive mild steel material is:

B (s^{-1}) = 6844

q = 3.91

<u>Dimensions and properties of external ring</u>

Yield strength, σ_0 = 361.322 MPa

Thickness, t = 2mm

Outer diameter, D = 42.3mm

Radius, R = 21.15 mm

Width = 10 mm

<u>Dimensions and properties of internal ring</u>

Yield strength, σ_0 = 361.322 MPa

Thickness, t = 2mm

Outer diameter, D = 15.9mm

Radius, R = 7.95 mm

Width = 10 mm

Sample calculation for multi-ring sample 1 (8kg, 500mm)

<u>External ring</u>

Initial velocity, *V* = $\sqrt{2\ x\ 9.81\ x\ 0.5}$

= 3.1321 m/s

Strain rate, $\dot{\varepsilon} = \frac{3.1321}{2(0.02115)}$

= 74.0449 s^{-1}

$$\frac{\sigma_{0d}}{361.322\ x\ 10^6} = 1 + \left(\frac{74{,}0449}{6844}\right)^{1/3.91}$$

Dynamic yield stress, σ_{0d} = 474.8567 MPa

Collapse load, P_0 (external) = $\frac{(474.8567\ x\ 10^6)\ (0.002)^2}{(0.02115)}$

= 89807.41 N/m

= 89807.41 x 0.01

= 898.0741 N

<u>Internal ring</u>

$\dot{\varepsilon} = \frac{3.1321}{2(0.02115)}$

= 196.9874 s^{-1}

$$\frac{\sigma_{0d}}{361.322\ x\ 10^6} = 1 + \left(\frac{196.9874}{6844}\right)^{1/3.91}$$

σ_{0d} = 507.1395 MPa

Collapse load for 1 ring, P_0 (internal) $= \frac{(507.1395\ x\ 10^6)(0.002)^2 \cot[(\pi + 60°)]/8}{0.00795}$

= 9885.07 N/m

= 9885.07 x (10 x 10^{-3})

= 98.8507 N

Total collapse load Σ P_0 = P_0 (external) + P_0 (internal)

= 898.0741 + (4 x 98.8507)

= 1293.4771N

Table 4.9 Experimental data and results for multi-ring under dynamic loading

Sample	**Mass (kg)**	**Height/ Stroke (mm)**	**Potential energy (J)**	**Initial velocity, V_0 (m/s)**	**Theoretical collapse load, P_0 (N)**	**Experimental collapse load, P_0 (N)**	**Percentage difference between theoretical and experimental collapse load (%)**
1	11.254	500	55.2	3.1321	1293.4771	1511.7330	14.44

2	11.254	500	55.2	3.1321	1293.4771	1135.0422	13.96
3	9.254	500	45.4	3.1321	1293.4771	1039.5693	19.63
4	13.254	380	49.4	2.7305	1348.1228	1348.1228	5.15
5	7.254	600	42.7	3.4310	1297.4408	1319.4557	1.70
6	8.254	630	51.0	3.5158	1303.3284	1486.4120	14.05

The experimental collapse load value is taken from the first peak of the graph (as shown from Figure 4.22 to Figure 4.27) before a significant/rapid change of displacement occurs. The average percentage error of collapse load between the theoretical and experimental for multi ring is 11%. The average experimental collapse load for multi ring under dynamic loading is 1307N and there is a percentage difference of 29% compared to the collapse load of multi ring under quasi-static loading. This is mainly because of the effect of strain rate or velocity per unit length subjected on the multi ring. The effect of strain rate could only be seen in dynamic loading and not in quasi-static loading since the loading rate of 2mm/min is low and there is no significant strain rate effect that could be seen.

The graphs shown from Figure 4.22 to Figure 4.27 are the graphs of load versus displacement for multi ring under dynamic loading and it is plotted until the densification zone at displacement 26.2958 mm. Graphs plotted were only until the densification zone. Area under the graph shows the useful energy that could be absorbed by the multi ring under dynamic loading. The useful energy absorbed by the ring is tabulated in Table 4.10. If the area of graph was to be included till the densification zone (Figure 4.22), the total energy absorbed would be almost similar with the potential energy dissipated onto the multi ring structure. The area under the curve for graph on Figure 4.22 is 58.58 J and the potential energy for multi ring 1 is 55.2 J.

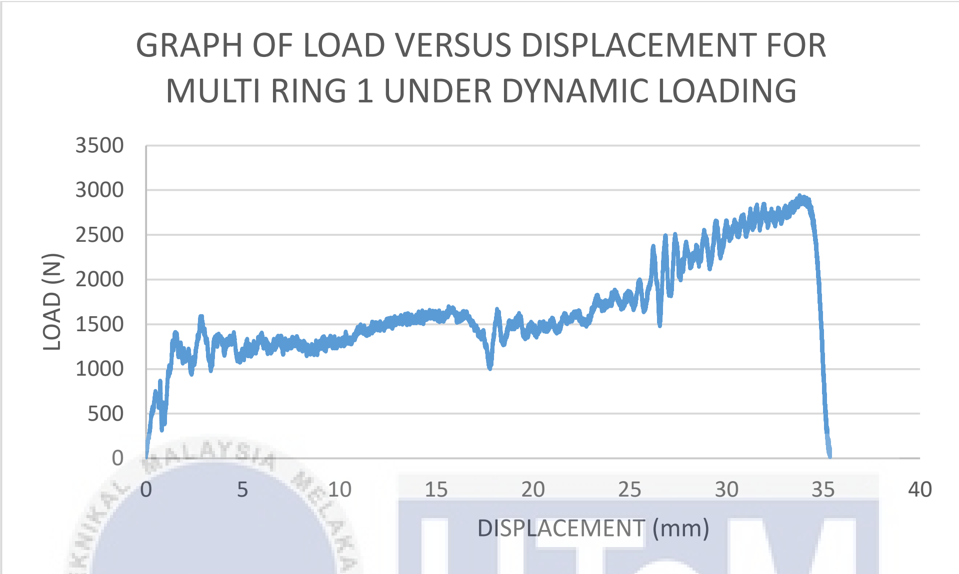

Figure 4.22 Graph of load versus displacement for multi ring 1 under dynamic loading

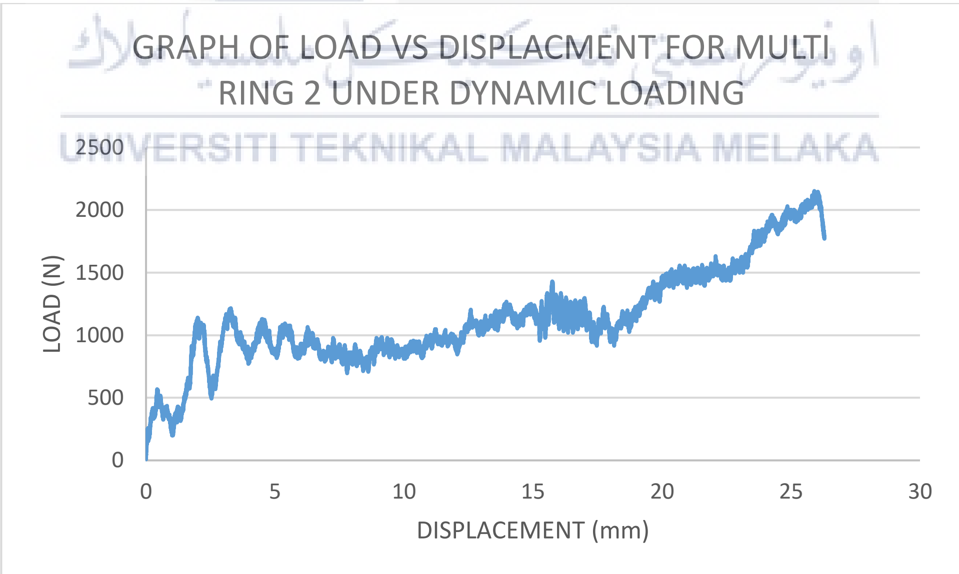

Figure 4.23 Graph of load versus displacement for multi ring 2 under dynamic loading

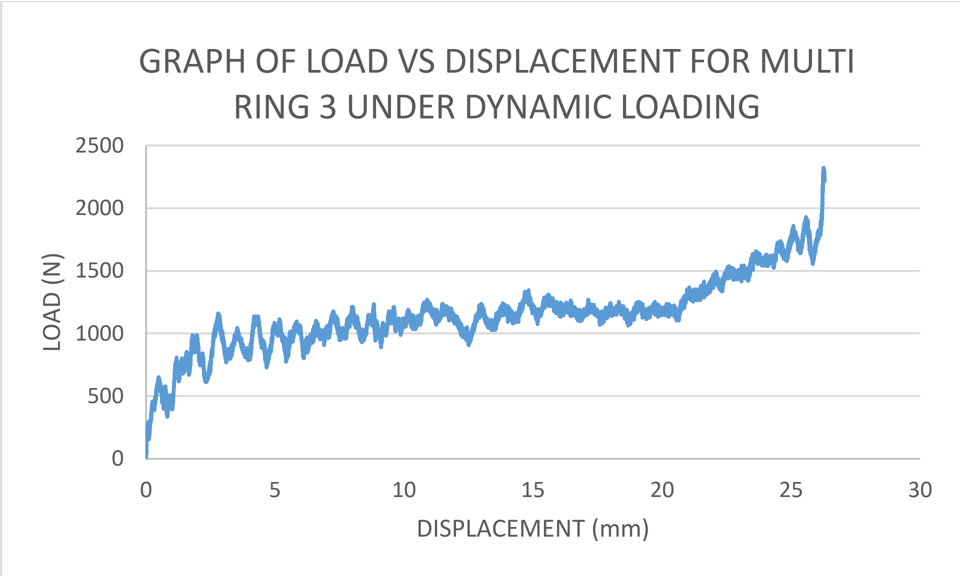

Figure 4.24 Graph of load versus displacement for multi ring 3 under dynamic loading

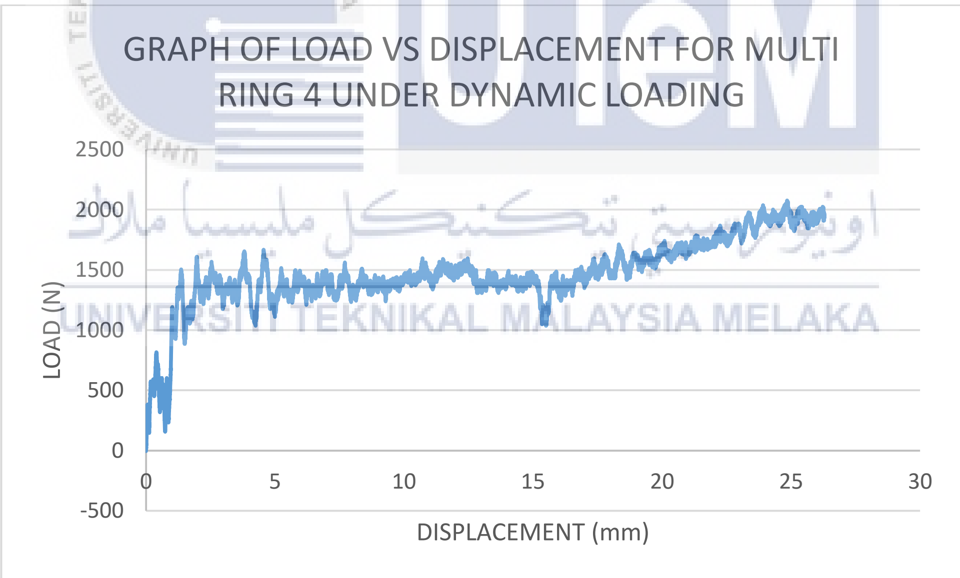

Figure 4.25 Graph of load versus displacement for multi ring 4 under dynamic loading

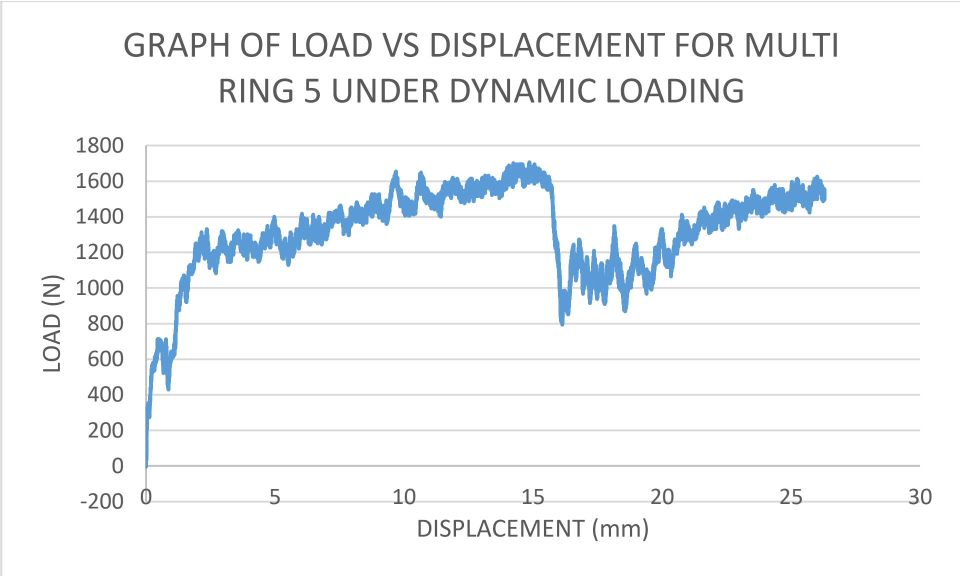

Figure 4.26 Graph of load versus displacement for multi ring 5 under dynamic loading

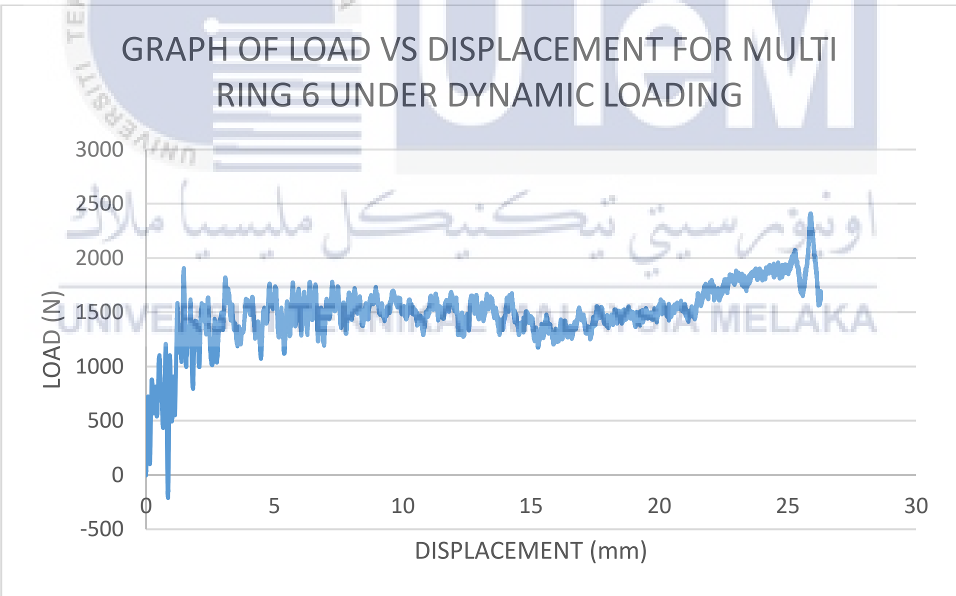

Figure 4.27 Graph of load versus displacement for multi ring 6 under dynamic loading

The average energy absorbed by the multi ring under dynamic loading is 34913.07 Nmm or 34.91 J. Figure 4.28 shows the images of multi ring subjected to impact which it was recorded in a high-speed camera with each image displaying the frame recorded and time of contact in milliseconds.

Table 4.10 Energy absorbed by multi ring under dynamic loading

Useful energy absorbed /	**Area under the graph until plateau zone**
Sample 1	37004.06 Nmm
Sample 2	29839.97 Nmm
Sample 3	30102.61 Nmm
Sample 4	38582.95 Nmm
Sample 5	34695.57 Nmm
Sample 6	39253.26 Nmm
Average energy absorbed	*34913.07 Nmm*

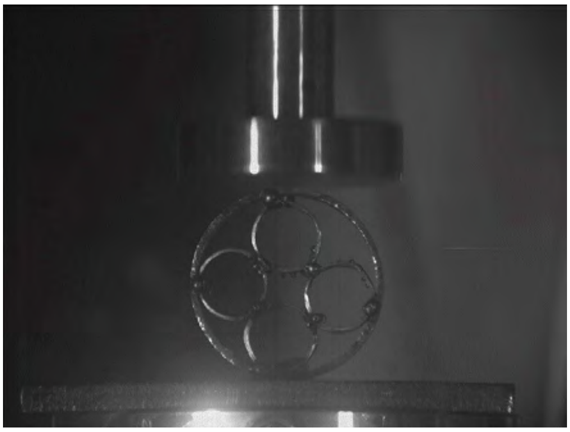

Frame 1:0ms

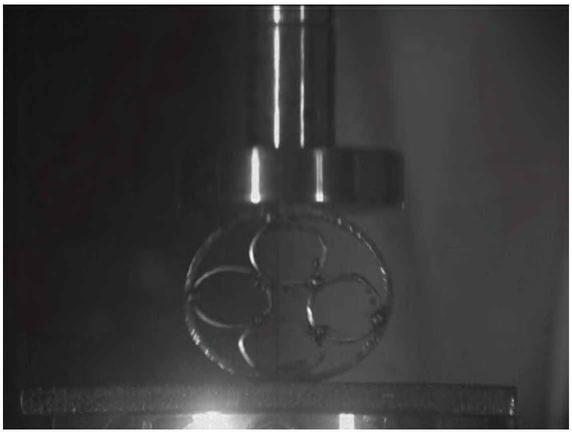

Frame 3:2ms

Frame 5:4ms

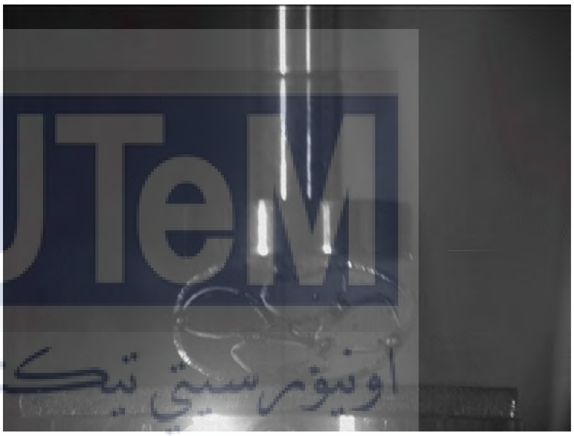

Frame 7:6ms

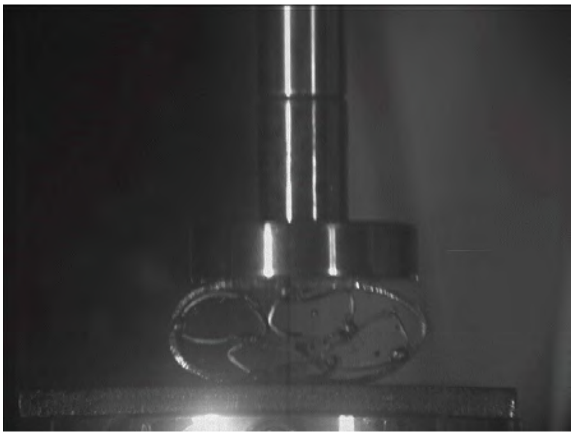

Frame 9:8ms

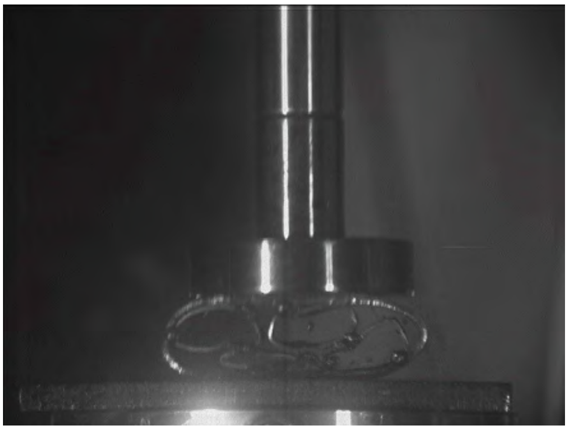

Frame 11:10ms

Frame 13:12ms Frame 15:14ms

Figure 4.28 Displacement of multi ring under dynamic loading

Figure 4.29 shows the superimposed graph multi ring and singular ring subjected to dynamic loading and quasi-static loading. The area under the curve is the total useful energy absorption capacity. It clearly shows that multi ring (subjected to dynamic loading and quasi-static loading) holds an advantage than single ring (subjected to dynamic loading and quasi-static loading) since it has a higher energy absorption capacity and collapse load value. It has been proven that the addition of internal rings could increase the energy absorption of a ring subjected to lateral loading.

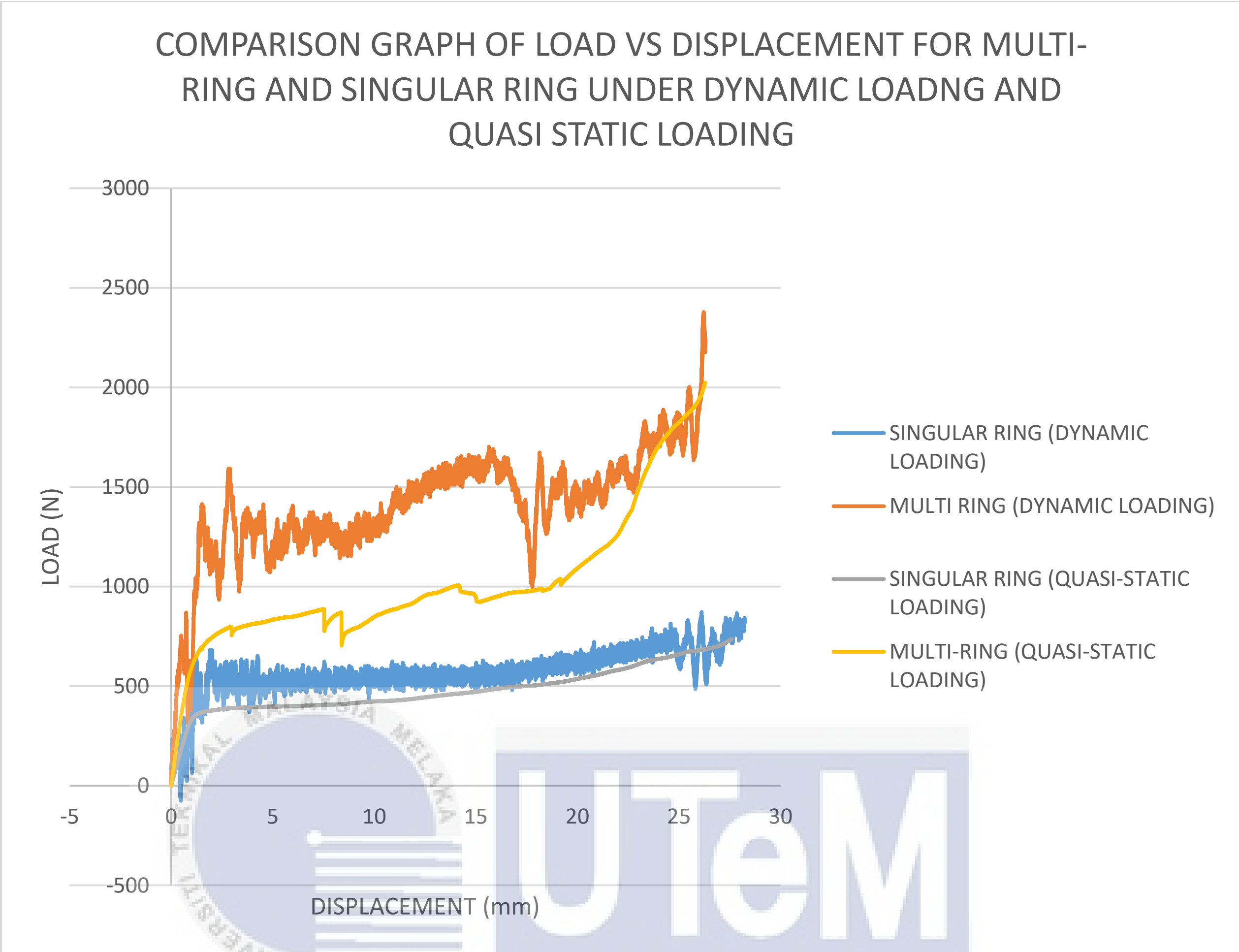

Figure 4.29 Superimposed graph of singular ring and multi ring subjected to quasi-static loading and dynamic lo ading

CHAPTER 5

CONCLUSION AND RECOMMENDATION

5.1 Conclusion

From the experimental works carried out for quasi-static loading and dynamic loading, it was proven that the multi-ring holds a greater advantage than a single ring when it was laterally loaded. This is because the multi-ring has a higher energy absorbing capacity and a higher collapse load (transition point before significant deformation occurs) value. This also means that the multi-ring is able to withstand a higher amount of force before entering the plateau zone. Based on Eq(11), it is proven that the deformation increases as the lateral load subjected on a ring increases, but the useful energy that could be absorbed by the structure is only till the plateau zone. For quasi-static loading, the multi-ring has an energy absorbing capacity of 31.02J and 14.18J for single ring. On the hand, due to effects of strain rate the multi-ring under dynamic loading has an energy absorbing capacity of 34.91J and 16.00J for single ring. This proves that the addition of internal ring could increase the energy absorbing capacity of a ring subjected to lateral loading. This could then be applied as an impact energy absorbing device in reducing the impact subjected on a structure which could ensure the safety of the human in that structure.

5.2 Recommendation

Welding method would not be an appropriate method in joining the internal rings with the external ring due to the formation of burrs on the rings. These burrs could highly effect the performance of the multi-ring where sudden fluctuations in the load versus displacement could be seen. Since this method requires high skills of the welder, other method such as using a metal glue in joining the rings should be used in the future research works.

Besides that, it is also recommended that further experimental works should be carried out in obtaining the material strain rate sensitivity (constant of B and q) since the existing Copper-Symonds constant are used only for material with small strains.

REFERENCES

A.ALaviNia, & S.Chahardoli. (2016). Optimizing tthe layout of nested three-tube structures in quasi-static. *Thin-walled structures*, 169-181.

A.Baroutaji, Gilchrist, M., & Olabi, A. (2016). quasi-static, impact and energy absorption of internally nested tubes subjected to lateral loading. *Thin-Walled Structures*, 337-350.

Alghamdi, A. (2000). Collapsible impact energy absorbers: an overview. *Thin-walled structures*, 189-213.

Ambrósio, J. A., Pereira, M. F., & Silva, F. P. (1996). *Crashworthiness of transportation system: Structural impact and occupant protection.* Lisboa: Springer-Science+Business Media,B.V.

Baroutaji, A., Gilchrist, M., Smyth, D., & Olabi, A. (2015). Crush analysis and multi-objective optimization design for circular tube under quasi-static lateral loading. *Thin-Walled Structures*, 121-131.

Chung, Y.-W. (2007). *Introduction to material science and engineering.* Boca Raton: CRC Press.

G.Lu, & T.X.Yu. (2003). *Energy absorption of structures and materials.* Cambridge: Woodhead Publishing Limited.

Gold, V. (1987). *Compendium of Chemical Terminology.* Blackwell Scientific Publications.

Jones, N. (1989). *Structural Impact.* Cambridge: Cambridge University Press.

Khalil, Z. B., Yamashita, M., Kuno, Y., & Hattori, T. (2014). Energy absorption performance of press-formed shell . *Procedia Engineering*, 951-956.

Li, Z., Zheng, Z., Yu, J., & Guo, L. (2013). Crashworthiness of foam-filled thin-walled circular tubes under dynamic bending. *Materials and Design*, 1058-1064.

Moosbrugger, C. (2002). *Atlas of Stress-strain curves.* United States of America: ASM International.

Morris, E., Olabi, A., & Hashmi, M. (2006). Lateral crushing of circular and non-circular tube systems under quasi-static conditions. *Journal of Materials Processing Technology*, 132–135.

Murray, G. (1997). *Handbook of materials selection for engineering applications.* California: Marcel Dekker, Inc.

Olabi, A., Morris, E., Hashmi, M., & Gilchrist, M. (2008). Optimised design of nested circular tube energy absorbers under lateral impact loading. *International Journal of Mechanical Sciences*, 104-116.

REDDY, T. Y., & REID, S. R. (1978). LATERAL COMPRESSION OF TUBES AND TUBE SYSTEM WITH SIDE CONSTRAINTS . *International Journal of Mechanical Sciences,* , 187-199.

REID, S. R., & DREW, S. L. (1983). ENERGY ABSORBING CAPACITIES OF. *International Journal of Mechanical Sciences*, 649-667.

Tran, T. (2016). Crushing analysis of multi-cell thin-walled rectangular and square tubes. *Composite Structures*, 734-747.

Zhang, Z.-X. (2016). *Rock Fracture and Blasting Theory and Applications.* Svalbard: Elsevier Inc.

APPENDIX

APPENDIX A1

Gantt chart for semester 1

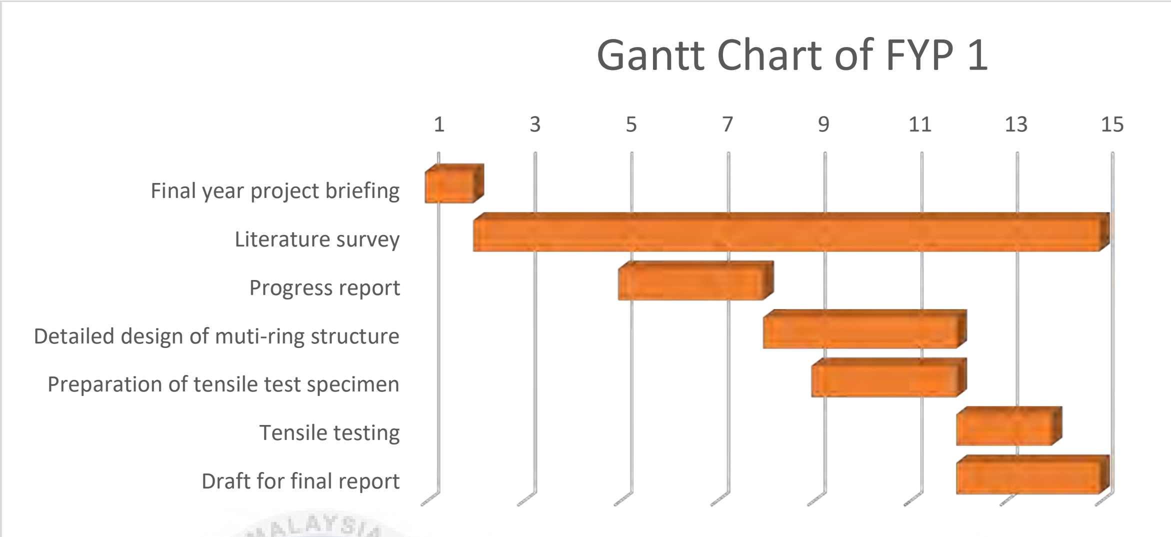

APPENDIX A2

Gantt chart for semester 2